PART IX

RECEPTOR-RECYCLING MODEL OF CLEARANCE AND DISTRIBUTION OF INSULIN IN THE PERFUSED MOUSE LIVER

SUMMARY

After perfusion of mouse livers with A_{14}-^{125}I-insulin for designated intervals, an acid-wash technique was employed to separately measure the surface-bound (X_s) and intracellular (X_i) A_{14}-^{125}I-insulin, as well as intracellular degradation products (X_{deg}) of labeled insulin. From the perfusate concentrations (C_p) of A_{14}-^{125}I-insulin, the apparent intrinsic hepatic clearance of labeled insulin at a high dose (0.2 nmol/l) was shown to be 60% smaller than that at a low dose (0.018 nmol/l), indicating that the cellular uptake of insulin is remarkably nonlinear at the concentration range examined. From the time courses of C_p, X_s, X_i and X_{deg}, the hepatic insulin disposition was shown to be largely accounted for by the receptor-mediated endocytosis. The observed data at the low dose were analyzed to estimate biochemical parameters, (i.e., total receptor number, endocytotic rate constant and intracellular degradation rate constant) according to "receptor-recycling" and "non-receptor-recycling" models, using a computer-aided optimization procedure. The "receptor-recycling" model could not only adequately explain the C_p, X_s, X_i and X_{deg} at the low dose, but also predict the C_p at the high dose. On the other hand, a "non-receptor-recycling" model, in which recycling of receptors was not assumed, could also explain the observed data at the low dose, but failed to predict the C_p at the high dose, indicating that the receptor recycling process is necessary to explain the hepatic insulin clearance at high insulin concentrations, at which hepatic insulin clearance should be limited by the rate of receptor recycling. However, the applicability of our model might be limited within the physiologic insulin concentrations, because of the negative cooperativity of insulin-receptor interaction and a high-capacity, nondegradative and more rapidly recycling pathway for receptors that may occurs at high concentrations of insulin. In conclusion, we developed a mathematical model of hepatic insulin clearance and distribution under physiological conditions, including receptor binding, receptor-mediated endocytosis and receptor recycling, which have been so far demonstrated using isolated hepatocytes.

INTRODUCTION

There is a growing body of evidence that various polypeptides are taken up by their target cells *via* receptor-mediated endocytosis [1,2]. In particular, the uptake of insulin by isolated hepatocytes involves binding to receptors, endocytosis of insulin-receptor complex, dissociation of the ligand from the receptor in an acidified endosomal compartment, and transport of the ligand to the lysosomes in which the ligand is degraded [3]. On the other hand, the internalized insulin receptors are largely recycled back to the surface of hepatocytes and reutilized [3,4].

The liver plays a major role in regulating the peripheral insulin concentration due to extraction of insulin from the portal blood before entrance into the systemic circulation. Therefore, there have been a number of reports to measure hepatic extraction of insulin in *in vivo* and in isolated perfused livers, which demonstrate a nonlinear hepatic clearance at physiological insulin concentrations [5-7]. Moreover, it has been proposed that receptor-mediated endocytosis and its subsequent events such as receptor recycling are the major mechanisms by which receptor down-regulation is mediated [8-10]. However, there have been no explicit approaches to predict the changes in hepatic clearance and distribution of insulin, as well as the changes in surface receptor number in a physiological situation, possibly due to the lack of an adequate kinetic model.

Therefore, in the present study, we performed mouse liver perfusion experiments to examine hepatic clearance and distribution of A_{14}-^{125}I-insulin, combined with an acid-wash technique [11,12] to separately measure the surface-bound and internalized amounts of A_{14}-^{125}I-insulin, and intracellular degradation products of A_{14}-^{125}I-insulin in

the liver. In order to analyze the observed data, we developed an organ model of hepatic insulin disposition, including receptor binding, receptor-mediated endocytosis and receptor recycling, namely the "receptor-recycling" model. Using this model, we attempted to predict the nonlinear hepatic elimination of insulin and the down-regulation of surface insulin receptors in the liver. The importance of receptor recycling on the hepatic insulin clearance was also discussed.

MATERIALS AND METHODS

Materials. Human insulin ^{125}I-labeled at tyrosine-A_{14} (A_{14}-^{125}I-insulin), with a specific activity of 2000 Ci·mmol^{-1}, was purchased from Amersham International Ltd. (Buckinghamshire, UK). Crystalline porcine insulin and bovine serum albumin (BSA; Fraction V) were obtained from Sigma Chemical Co. (St. Louis, MO, USA), and trichloroacetic acid (TCA) from Wako Pure Chemical Industries, Ltd. (Osaka, Japan). Bovine erythrocytes were kindly supplied from the Meat Inspection Center of Kanazawa City (Ishikawa, Japan). All other reagents were commercially available and of analytical grade. The labeled insulin was dissolved in phosphate buffered saline (PBS) containing 0.1% BSA and stored at -20°C until study. The labeled insulin used was at least 98% pure as assayed by both TCA-precipitability and HPLC analysis.

Animals. Adult male ddY mice were obtained from Sankyo Laboratory Co., Ltd. (Toyama, Japan) and allowed free access to standard rodent chow and water. Mice were fasted overnight before use.

In Situ Liver Perfusion. Mice were anesthetized with intraperitoneal pentobarbital (50mg·kg^{-1}), and livers were operated according to the method of Mortimore [13]. The livers were cyclically perfused *in situ* at 37°C in a temperature-controlled cabinet. The perfusate consisted of 10% washed bovine erythrocytes, 3% BSA, and 3.69 mmol/l glucose in Krebs-Ringer bicarbonate (KRB) buffer (pH 7.4). Perfusate was continuously oxygenated with 95% O_2/5% CO_2 by passage through silastic tubing in an oxygenation chamber. The inlet temperature was kept at 37°C. After operation, livers were perfused with erythrocyte-free KRB buffer in a single-pass system for 5 min, and perfused with 12.0 ml erythrocyte-containing KRB buffer in a

closed-circuit system for 10-min. Then, a tracer amount of A_{14}-^{125}I-insulin (0.44μCi or 0.018 nmol/l in a final concentration), with and without 2 nmol/l of unlabeled insulin, was added in the reservoir which was constantly stirred. Subsequently, portions (100 μl) of the perfusate were sampled at designated times, and centrifuged for 1 min in a microcentrifuge to remove erythrocytes. A_{14}-^{125}I-insulin in perfusate samples (without erythrocytes) was assayed by either TCA-precipitation or HPLC analysis as described later. Unless otherwise mentioned, the perfusion flow rate (including erythrocytes) was set at 1.85 ml·min^{-1} and the perfusion pressure at 15-18 mmHg, using a peristaltic pump (model MP, Tokyo Rikakikai Co, Tokyo, Japan). During the 30-min perfusion, the concentrations of glutamic oxaloacetatic transaminase (GOT) and glutamic pyruvic transaminase (GPT) were determined with a commercial test kit (STA-Test Wako, Wako) to assess the viability of the perfused livers.

Acid-Wash Technique in the Perfused Liver. At designated times after the addition of A_{14}-^{125}I-insulin into the reservoir, the acid-wash technique was performed as previously described [12]. After twenty fractions of acid-washout solution (designated as acid samples) containing acid-extractable radioactivity were sequentially collected, livers were quickly removed and a 1-g portion of each liver was homogenized in 4 ml of ice-cold 1 mol/l acetic acid containing 6 mol/l urea. The remaining portion of the liver was weighed and counted for the total radioactivity in a γ-counter (model ARC-300, Aloka Co., Ltd., Tokyo, Japan). The tissue homogenates containing acid-resistant radioactivity were then centrifuged at 3000 rpm for 15 min in a centrifuge (model RL-500SP, Tomy Seiko Co., Ltd., Tokyo, Japan) at

4°C, and the obtained supernatants (designated as tissue samples) were transferred to separate tubes for the assay of A_{14}-^{125}I-insulin. The percentage of radioactivity recovered in the tissue samples was more than 90%.

Analytical Methods. For the TCA-precipitation method, perfusate samples (80 µl), acid samples (2.5 ml per fraction) or tissue samples (4 ml) were mixed well with 5% TCA solution in a final concentration, kept standing at 4°C for 30 min, and centrifuged at 3000 *g* for 15 min. For acid samples, 50 µl of perfusate (containing 3% BSA) was added to the mixture as a precipitation carrier. The supernatants were transferred into separate tubes by aspiration. The radioactivity in the precipitates and supernatants was measured in a γ-counter.

For the HPLC analysis, each sample was deproteinized by mixing vigorously with an equal volume of ethanol, and centrifuged at 10000 *g* for 5 min in a microcentrifuge (MR-15A, Tomy Seiko Co.) at 4°C. The ethanol-treated supernatants were filtered through 0.45-µm millipore filters (type HV; Nihon Millipore Kogyo, Yonezawa, Japan) with the recovery of more than 80%. The resultant filtrates (100 µl) were loaded onto a reversed-phase HPLC column, µ-Bondapak C_{18} (30 cm x 3.9 mm i.d., Waters Associates, Inc., Milford, MA, USA). The eluents were collected automatically and the radioactivity in each fraction (1.0 ml) was measured in a γ-counter. The solvent delivery system, equipments, mobile phase, and elution condition are the same as described previously [12].

"Receptor-Recycling" Model. Considering a liver perfusion in a recirculation system, we developed an organ model of hepatic insulin clearance and distribution, in which insulin receptors are transferred between cell surface and intracellular (vesicular) space. The

structure of the model is shown in Fig. 1. The differential equations describing the system are given as follows:

$$\frac{dR_s}{dt} = k_{ret} \cdot R_i - k_{end} \cdot X_b - k_{sp} \cdot (R_s - X_b) \quad \text{(Eq.1)}$$

$$\frac{dR_i}{dt} = k_{end} \cdot X_b + k_{sp} \cdot (R_s - X_b) - k_{ret} \cdot R_i \quad \text{(Eq.2)}$$

$$V_p \frac{dC_p}{dt} = Q_p \cdot (C_e - C_p) \quad \text{(Eq.3)}$$

$$V_e \frac{dC_e}{dt} = Q_p \cdot (C_p - C_e) - k_{on} \cdot (R_s - X_b) \cdot f_p \cdot C_e + k_{off} \cdot X_b \quad \text{(Eq.4)}$$

$$\frac{dX_b}{dt} = k_{on} \cdot (R_s - X_b) \cdot f_p \cdot C_e - k_{off} \cdot X_b - k_{end} \cdot X_b \quad \text{(Eq.5)}$$

$$\frac{dX_i}{dt} = k_{end} \cdot X_b - k_{deg} \cdot X_i \quad \text{(Eq.6)}$$

$$\frac{dX_{deg}}{dt} = k_{deg} \cdot X_i - k_{rel} \cdot X_{deg} \quad \text{(Eq.7)}$$

where f_p denotes the fraction of insulin unbound to albumin in the perfusate. During the intracellular degradation products are not yet released substantially (i.e., $k_{deg}\ X_i << k_{rel}\ X_{deg}$), Eq.7 can be approximated to:

$$\frac{dX_{deg}}{dt} = k_{deg} \cdot X_i \quad \text{(Eq.8)}$$

Data Analysis. The values of X_s, X_i and X_{deg} were expressed as intact A_{14}-^{125}I-insulin (pmol per g liver), and C_p also as intact A_{14}-^{125}I-insulin (pmol per ml perfusate). The hepatic clearance (CL_H) of A_{14}-^{125}I-insulin was calculated as follows:

$$CL_H = k_e \cdot V_p / LW \quad \text{(Eq.9)}$$

where k_e is the exponential slope of the disappearance of A_{14}-^{125}I-insulin in the perfusate, and LW is the liver weight in grams. Based on the clearance theory [14], the CL_H is a function of Q_p and the apparent intrinsic activity of hepatic elimination, $CL_{int,app}$ [14]. The $CL_{ins,app}$ is given by:

$$CL_{int,app} = \frac{Q_p \cdot CL_H}{(Q_p - CL_H)f_p} \qquad \text{(Eq.10)}$$

Determination of Kinetic Parameters. Since our preliminary simulation indicated that k_{end}, k_{deg} and R_T are important parameters that determine the time courses of C_p, X_s, X_i and X_{deg} at a tracer dose, these three parameters were optimized by a procedure as described later. The other parameters (i.e., V_e, V_p, Q_p, f_p, k_{on}, k_{off}, k_{sp} and k_{ret}) were measured experimentally, cited or calculated from published references (Table 2). For optimization of kinetic parameters, a nonlinear least-squares regression analysis, NONLIN74 [16], was used throughout this study on a digital computer (FACOM-M360AP) at the Information Processing Center, Kanazawa University. In particular, k_{sp} and k_{ret} were calculated from published data using the methods described as follows:

Calculation of k_{sp}. The apparent endocytotic rate constant ($k_{end,app}$) can be expressed as:

$$k_{end,app} = v \cdot k_{end} + (1 - v) \cdot k_{sp} \qquad \text{(Eq.11)}$$

where v is the fraction of surface receptors occupied by insulin and given by:

$$v = \frac{C_e}{K_d + C_e} \qquad \text{(Eq.12)}$$

The values of k_{sp} and k_{end} were obtained by a nonlinear least-squares regression analysis according to Eq.11, based on the concentration-dependent $k_{end,app}$ values observed in isolated rat hepatocytes [11].

Calculation of k_{ret}. Using v, Eq.1 can be written as follows [17]:

$$\frac{dR_s}{dt} = k_{ret} \cdot (R_T - R_s) - [v \cdot k_{end} + (1 - v) \cdot k_{sp}] \cdot R_s \qquad \text{(Eq.13)}$$

Since most of the mobile receptors are considered to be located at the surface of hepatocytes in fasted rats (i.e., $v \doteq 0$), R_T can be expressed as follows, under the steady-state basal condition (i.e., $dR_s/dt = 0$ in Eq.13):

$$R_T = \frac{k_{sp} + k_{ret}}{k_{ret}} R'_{s,0} \qquad \text{(Eq.14)}$$

where $R'_{s,0}$ represents the R_s under the steady-state basal condition in fasted rats. On the other hand, when nonfasted rats received an intraportal injection of a large excess of unlabeled insulin (i.e., $v = 1$), Eq.13 can be transformed to:

$$\frac{dR_s}{dt} = k_{ret} \cdot R_T - (k_{ret} + k_{end}) \cdot R_s \qquad \text{(Eq.15)}$$

Integration of Eq.15 from time 0 to t and rearrangement gives:

$$\ln \frac{R_{s,0} - R_{s,eq}}{R_s - R_{s,eq}} = (k_{ret} + k_{end}) \cdot t \qquad \text{(Eq.16)}$$

where $R_{s,0}$ and $R_{s,eq}$ are the surface receptor numbers at the initial and equilibrium states, respectively, in nonfasted rats injected with intraportal dose of unlabeled insulin; and $R_{s,eq}$ is expressed as:

$$R_{s,eq} = \frac{k_{ret}}{k_{end} + k_{ret}} R_T \qquad \text{(Eq.17)}$$

Substitution for R_T in Eq.17 according to Eq.14 gives:

$$R_{s,eq} = \frac{k_{sp} + k_{ret}}{k_{end} + k_{ret}} R'_{s,0} \qquad \text{(Eq.18)}$$

Solving Eq.16 for $R_s/R_{s,0}$ and rearrangement using Eq.18 yields:

$$\frac{R_s}{R_{s,0}} = (1 - \alpha)\cdot\exp[-(k_{ret} + k_{end})\cdot t] + \alpha \qquad \text{(Eq.19)}$$

where α is expressed as:

$$\alpha = \frac{k_{ret} + k_{sp}}{k_{ret} + k_{end}} \cdot \frac{R'_{s,0}}{R_{s,0}} \qquad \text{(Eq.20)}$$

According to the report by López and Desbuquiois [10], the $R'_{s,0}/R_{s,0}$ value is 1.1, indicating that the R_s in fasted rats is slightly (10%) higher than that in fed rats. Therefore, one can estimate the k_{ret} and k_{end} values by fitting the reported $R_s/R_{s,0}$ *vs* time curve (i.e., *in vivo* down-regulation) to Eq.19, using a nonlinear least-squares regression analysis.

In order to optimize the R_T, k_{end} and k_{deg}, the observed data on C_p (0-30 min), X_s, X_i (0-20 min) and X_{deg} (0-5 min) at the tracer dose (0.018 nmol/l) were fitted to the simultaneous differential equations (Eqs.1-6 and 8) by a nonlinear least-squares regression analysis. Moreover, in order to examine the effect of receptor recycling on hepatic insulin clearance, the observed data were also fitted to the simultaneous differential equations of a "non-receptor-recycling" model, in which k_{ret} is set at zero.

Since the initial value of k_{end}, k_{deg} and R_T are required for the above-mentioned optimization procedure, the following methods were employed for the estimation of respective initial values.

Initial estimation of k_{end}. Summation of both hand sides of Eqs.6 and 8 gives:

$$\frac{d(X_i + X_{deg})}{dt} = k_{end}\cdot X_b \qquad \text{(Eq.21)}$$

Therefore, the integration of Eq.21 from time 0 to t gives:

$$X_i + X_{deg} = k_{end}\cdot\int_0^t X_b dt \qquad \text{(Eq.22)}$$

where $\int_0^t X_b dt$ was calculated numerically by a trapezoidal rule. Then, a plot of $(X_i + X_{deg})$ *vs.* $\int_0^t X_b dt$ should give a straight line passing through the origin, and the slope of the plot should yield an initial estimate of k_{end}.

Initial estimation of k_{deg}. The integration of Eq.8 from time 0 to t gives:

$$X_{deg} = k_{deg}\cdot\int_0^t X_i dt \qquad \text{(Eq.23)}$$

where $\int_0^t X_i dt$ was calculated numerically by a trapezoidal rule. Then, a plot of X_{deg} *vs.* $\int_0^t X_i dt$ should give a straight line passing through the origin, and the slope of the plot should yield an initial estimate of k_{end}.

Initial estimation of R_T. When a ligand is taken up *via* receptor-mediated endocytosis, the $CL_{int,app}$ of the ligand is expressed as follows, under a linear condition (i.e., at a tracer dose) [18]:

$$CL_{int,app} = \frac{k_{on}\cdot R_s\cdot k_{end}}{k_{end} + k_{off}} \qquad \text{(Eq.24)}$$

Eq.24 gives an initial estimate of R_s, by substituting the reported values of k_{on} and k_{off} (Table 2), the graphical estimate of k_{end} calculated by Eq.22, and the $CL_{int,app}$ calculated by Eq.10. The initial estimate of R_s was considered as that of R_T, because most of the mobile receptors should be located at the cell surface when a tracer dose of insulin was added in the perfused liver.

Prediction of the time course of C_p at a high dose (2 nmol/l). Using the values of R_T, k_{end} and k_{deg} estimated above at the low dose,

both the "receptor-recycling" and "non-receptor-recycling" models were employed to predict the disappearance of A_{14}-^{125}I-insulin from the perfusate at a high dose (2 nmol/l) to test the feasibility of these models. Two nanomolar was chosen as a high concentration of insulin, since portal insulin concentrations in the postabsorptive state were reported to be 0.4-1.1 nmol/l [5].

RESULTS

In Situ Liver Perfusion. Livers were perfused *via* the portal vein at a constant physiological pressure with a perfusate containing 10% erythrocytes as an oxygen carrier, and there was no appearance of edema during the experiment. The characteristics of the perfused mouse livers are summarized in Table 1. The perfusion flow rate and perfusion pressure were constant during the experiments. The releasing rates of GOT and GPT are close to that of GOP reported in normal rat livers [19]. Taken together, the viability of the livers was judged to be normal and constant.

Figures 2A-2E show typical HPLC profiles of ^{125}I-radioactivity collected from the reservoir perfusate at 0, 10, 15, 20, and 30 min. The total radioactivity eluted from the column was almost 100% of the radioactivity loaded onto the column. A small peak eluting at 3-4 min probably represents a mixture of $^{125}I^-$ and monoiodotyrosine, because a standard 3-I-L-tyrosine eluted as early as 3.9 min and very close to the salt peak (3.1 min) under the present analytical condition. The retention time of intact A_{14}-^{125}I-insulin was 20 min, and it was clearly seen that A_{14}-^{125}I-insulin was extensively metabolized by the mouse liver during the perfusion. The identity of a small peak eluting at 16 min (seen in the profiles of the perfusates samples at 10-20 min) is not clear from the present study, but it possibly represents intermediate degradation products of labeled insulin, because previous HPLC studies have demonstrated TCA-precipitable, insulin-sized intermediate products derived from enzymatic interactions of insulin with hepatocytes [20].

The relationship of the intactness of A_{14}-^{125}I-insulin in perfusate samples between the TCA-precipitation and HPLC-separation methods

(Fig. 3) indicates that the TCA-precipitation overestimates the intactness of A_{14}-^{125}I-insulin, as shown in a previous *in vivo* study [21], and further underestimates the hepatic insulin clearance. Moreover, correlation of intactness of A_{14}-^{125}I-insulin in the acid samples and tissue samples between the two methods was almost superimposed with the curve shown in Fig. 3 (not shown). Although HPLC analysis has a greater resolving power to differentiate between the intact peptide and its metabolites compared with other methods, it is very laborious to analyze many samples by HPLC. Therefore, we routinely employed the TCA-precipitation method, and the measured TCA-precipitability (%) was converted to the percentage of intact A_{14}-^{125}I-insulin on HPLC, using the correlation between these two methods.

Figure 4 shows the disappearance of A_{14}-^{125}I-insulin from the perfusate and the appearance of its degradation products in the perfusate, after the addition of a tracer amount of A_{14}-^{125}I-insulin in the reservoir.

Acid-Wash Technique in the Perfused Liver. When a liver was washed with ice-cold saline for 5 min and then with ice-cold acidic buffer for 20 min, two sharp peaks of ^{125}I-radioactivity representing the acid-extractable and acid-resistant A_{14}-^{125}I-insulin were sequentially eluted from the liver through the outflow cannula (Fig. 5). We analyzed some acid-extractable samples by HPLC and confirmed that more than 90% of the radioactivity represents intact A_{14}-^{125}I-insulin (result not shown).

Hepatic Clearance and Distribution of A_{14}-^{125}I-insulin. The time courses of C_p at low and high doses are shown in Fig. 6A. According to a linear regression analysis, the k_e values were determined to be

0.0739 $\pm$ 0.0017 and 0.0436 $\pm$ 0.0015 min^{-1} (mean $\pm$ SD) with the correlation coefficients (r) of -0.998 ($p < 0.001$) and -0.995 ($p < 0.001$) at low and high doses, respectively. These k_e values are significantly different from each other, as assessed by Student's t-test ($p < 0.001$). In a separate *in vitro* experiment, protein binding of A_{14}-^{125}I-insulin in the perfusate (KRB buffer containing 3% BSA) was examined using the polyethylene glycol precipitation method [22], and f_p was determined to be 1.0. Thus, the CL_H and $CL_{int,app}$ of A_{14}-^{125}I-insulin at these doses were calculated by Eqs.9 and 10, respectively, and are listed in Table 1. The $CL_{int,app}$ at the high dose was shown to be 60% smaller than that at the low dose, indicating that the cellular uptake of insulin is remarkably nonlinear at the concentration range examined.

Moreover, the time courses of acid-extractable and acid-resistant A_{14}-^{125}I-insulin, as well as that of acid-resistant degradation products of A_{14}-^{125}I-insulin at the tracer dose are shown in Fig. 6B.

Kinetic Analysis. The k_{sp} and k_{ret} values were determined to be 0.022 and 0.11 min^{-1} by Eq.11 and Eq.19, respectively (Table 2). Using Eqs.21 and 23, the initial estimates of k_{end} and k_{deg} were given as 0.655 $\pm$ 0.046 and 0.693 $\pm$ 0.024 min^{-1} (mean $\pm$ SD) with the r values of 0.998 ($p < 0.05$) and 0.999 ($p < 0.05$), respectively. Using Eq.24, the initial estimate of R_T was given as 11.1 pmol per liver. The R_T, k_{end} and k_{deg} were then optimized by fitting the observed data at the low dose (Fig. 6) to Eqs.1-6 and 8 using a nonlinear least-squares regression analysis, and are listed in Table 2.

The "receptor-recycling" model (Fig. 1) could adequately explain the hepatic clearance (Fig. 6A) and distribution (Fig. 6B) of A_{14}-^{125}I-

insulin at the low dose. The "non-receptor-recycling" model, in which no recycling of receptors (k_{ret} = 0) was assumed, could also simulate the observed data at the tracer dose, using another set of optimized parameters (i.e., k_{end}; 0.600 ± 0.036 min^{-1}, k_{deg}; 0.866 ± 0.058 min^{-1}, R_T; 9.93 ± 0.57 pmol per g liver, mean ± SD). On the other hand, a good prediction of the hepatic insulin clearance at the high dose was accomplished by the receptor-recycling model, but not by the non-receptor-recycling model (Fig. 6A).

Moreover, as can be inspected from Fig. 7, a computer-aided prediction using the receptor-recycling model at varying initial concentrations of insulin (C_p) suggests that the elimination rate constant (k_e) reduces dramatically at C_p > 1nmol/l, and that a marked reduction of surface receptors (i.e., "down-regulation") occurs also at C_p > 1 nmol/l.

DISCUSSION

Our kinetic model of hepatic insulin disposition includes several assumptions and approximations as described in the legends to Fig. 1. Unique to this model is the ability to predict the changes in surface receptor number in relation to extracellular insulin (Fig. 7B) as well. By use of this model, moreover, one could also examine quantitatively how the hepatic insulin clearance would be affected by variations in the affinity of insulin-receptor interaction, which may result from mutation of insulin receptor, abnormalities of insulin processing or mutation of insulin itself. However, the applicability of our model might be limited within the physiologic insulin concentratoins, because of the negative cooperativity of insulin-receptor interaction [23] and a high-capacity, nondegradative and more rapidly recycling pathway for receptors that occurs at high (supraphysiologic) concentrations of insulin [24].

Since about 50% of liver cells are not hepatocytes [25], there is a possibility that the observed clearance and distribution of A_{14}-^{125}I-insulin in the perfused livers are not due to specific interactions with hepatocytes. However, we could exclude this possibility, because the initial distribution of ^{125}I-insulin was limited to the hepatocyte plasmalemma after its intraportal injection [26,27], and its localization was diminished with simultaneous injection of excess unlabeled insulin [27].

In this study, an effective separation between the acid-extractable and acid-resistant A_{14}-^{125}I-insulin was performed by the acid-wash technique (Fig. 5). Moreover, our preliminary experiments showed that ^{125}I-radioactivity in both the acid-extractable and acid-resistant samples considerably decreased in the presence of 1 μmol/l unlabeled

insulin in the perfusate, and ^{125}I-radioactivity in the acid-resistant samples markedly decreased in the presence of 250 μmol/l of an endocytosis inhibitor, phenylarsine oxide (results not shown). These lines of evidence suggests that the observed acid-resistant A_{14}-^{125}I-insulin largely represents the intracellular A_{14}-^{125}I-insulin, and that the acid-extractable ^{125}I-radioactivity was bound to surface receptors.

As shown in Fig. 6, the peak of the intracellular A_{14}-^{125}I-insulin was several minutes later than that of surface-bound A_{14}-^{125}I-insulin, suggesting that the surface-bound ligand may be regarded as the substrate of endocytosis. Moreover, the increase of degradation products of A_{14}-^{125}I-insulin in the reservoir was small for the first 5 min, and rapidly increased thereafter. Since the lag time for A_{14}-^{125}I-insulin in the reservoir to reach the inlet of the organ was subtracted from the sampling time, this is not due to an access delay of A_{14}-^{125}I-insulin to the liver. Therefore, that the major site of insulin degradation is in an intracellular compartment but not in extracellular compartment is suggested in this study, as reported by other workers [28,29]. Taken altogether, the results obtained indicate that the hepatic insulin clearance is largely accounted for by the receptor-mediated endocytosis in the perfused mouse livers, and supports the feasibility of the present model of hepatic insulin clearance and distribution (Fig. 1).

As listed in Table 2, the value of R_T was estimated to be 8.66 pmol per g liver, that is 44000 sites per cell, assuming that the number of hepatocytes per liver in mice is the same as that in rats, 1.3×10^8 cells per g liver [30]. This R_T value is in good agreement

with the R_S for isolated rat hepatocytes *in vitro*, e.g., 45000 [31] and 50100 sites per cell [32], in which almost all mobile receptors may be located on the surface of isolated cells due to the absence of extracellular insulin during preparation. On the other hand, the estimated k_{end} is somewhat greater than that reported for isolated rat hepatocytes, 0.38 min^{-1} [24].

A good agreement between the observed and simulated values of C_p, X_s, X_i and X_{deg} at the low dose by both the receptor-recycling and non-receptor-recycling models (Fig. 6) suggests that internalization process, not receptor recycling, is important for the hepatic insulin clearance at low insulin concentrations. On the other hand, the predictions of C_p at the high dose by these models (Fig. 6A) suggest an important role of receptor recycling in the hepatic insulin clearance at high insulin concentrations, at which surface receptors are considered to be largely occupied. It follows to suggest that, when the R_S is considerably decreased at high insulin doses, the hepatic insulin clearance should be limited by the rate of receptor recycling. We propose, therefore, that the rate-limiting step of hepatic intrinsic clearance of insulin is the internalization process at low insulin concentrations, but moved to the receptor recycling process at relatively high concentrations. This is consistent with the fact that chloroquine, which blocks receptor recycling *via* preventing intravesicular acidification [2], did not alter the disappearance of A_{14}-^{125}I-insulin (tracer dose) in the perfused rat livers [33]. Thus, a dynamic "receptor-recycling" model could be advantageous to a static model of insulin clearance [34] that assumes a constant surface receptor number, because the latter model cannot evaluate the significance of receptor recycling on hepatic insulin

clearance. From the computer simulation (Fig. 7), it was predicted that the changes in the k_e (as well as CL_H) and R_s are not so sensitive to the initial concentrations of less than 1 nmol/l and more than 10 nmol/l, while very sensitive to those of 1-10 nmol/l. This is in agreement with the report that the hepatic extraction of insulin is reduced with increasing endogenous insulin secretion after pancreatic stimulation with oral glucose [35], when the portal vein insulin is reported to be 4.5-7.0 nmol/l [5]. However, further study should be focused on the validation of the model at a wider concentration range of insulin, and, if necessary, a more detailed modeling of hepatic insulin disposition should be performed to accomodate a full dose response curves as shown in Fig. 7A.

In conclusion, we have developed a "receptor-recycling" model of hepatic insulin clearance, based on a physiological and biochemical approach. The model could afford to predict not only the nonlinear clearance and distribution of insulin in the perfused liver, but also the change in surface receptor number, in a quantitative manner. The mathematical methods described here should be useful to analyze the receptor-mediated endocytosis of other ligands in an intact organ.

Acknowledgements. This study was supported by a Grant-in-Aid for Scientific Research from the Ministry of Education, Science and Culture of Japan, Project Research Fund from the Graduate School of Natural Science and Technology, Kanazawa University, and grants from the Nakatomi Foundation and Takeda Science Foundation.

REFERENCES

1. F. Gorden, J.L. Carpentier, JY. Fan, and L. Orci: Receptor mediated endocytosis of polypeptide hormones: mechanism and significance. *Metabolism* **31**, 664-669 (1982).
2. T. Wileman, C. Harding, and P. Stahl: Receptor-mediated endocytosis. *Biochem J.* **232**, 1-14 (1985).
3. O. Sonne: Receptor-mediated endocytosis and degradation of insulin. *Physiol. Rev.* **68**, 1129-1196 (1988).
4. M. Fehlman, J.L. Carpentier, E.V. Obberghen, P. Freychet, P. Thamm, D. Saunders, D. Brandenburg, and L. Orci: Internalized insulin receptors are recycled to the cell surface in rat hepatocytes. *Proc. Natl. Acad. Sci. USA* **79**, 5921-5925 (1982).
5. R.I. Misbin, T.J. Merimee, and J.M. Lowenstein: Insulin removal by isolated perfused rat liver. *Am. J. Physiol.* **230**, 171-177 (1976).
6. K.G. Tranberg: Hepatic uptake of isulin in man. *Am. J. Physiol.* **237**, E509-E518 (1979).
7. K. Polonsky, J. Jaspan, D. Emmanouel, K. Holmes, and A.R. Moossa: Differences in the hepatic and renal extraction of insulin and glucagon in the dog: evidence for saturability of insulin metabolism. *Acta Endocrinol.* **102**, 420-427 (1983).
8. M. Krupp and M.D. Lane.: On the mechanism of ligand-induced down-regulation of insulin receptor level in the liver cell. *J. Biol. Chem.* **256**, 1689-1694 (1981).
9. B. Desbuquois, S. Lopez, and H. Burlet: Ligand-induced translocation of insulin receptors in intact rat liver. *J. Biol. Chem.* **257**, 10852-10860 (1982).
10. S. López and B. Desbuquois: Insulin-related changes in the

subcellular distribution of insulin receptors in intact rat liver: Effects of acute hypoinsulinemia induced by diazoxide, somatostatin, and xylazine. *Endocrinology* **120**, 1695-1702 (1987).

11. B. Draznin, M. Trowbridge, and L. Ferguson: Quantitative studies of the rate of insulin internalization in isolated rat hepatocytes. *Biochem. J.* **218**, 307-312 (1984).
12. H. Sato, K. Yoshioka, T. Terasaki, and A. Tsuji: Receptor-mediated endocytosis of A14-^{125}I-insulin by the nonfiltering perfused rat kidney. *Biochim. Biophys. Acta* **1073**, 442-450 (1991).
13. G.E. Mortimore and F. Tietze: Studies on the mechanism of capture and degradation of insulin-I^{131} by the cyclically perfused rat liver. *Ann. New York Acad. Sci.* **82**, 329-337 (1959).
14. G.R. Wilkinson and D.G. Shand: A physiological approach to hepatic drug clearance. *Clin. Pharmacol. Ther.* **18**, 377-390 (1975).
15. H. Sato, Y. Sugiyama, S. Miyauchi, Y. Sawada, T. Iga, and M. Hanano: A simulation study on the effect of a uniform diffusional barrier across hepatocytes on drug metabolism by evenly and unevenly distributed uni-enzyme in the liver. *J. Pharm. Sci.* **75**, 3-8 (1986).
16. C.M. Metzler, G.L. Elfring, and A.J. McEwen: A package of computer programs for pharmacokinetic modeling. *Biometrics* **30**, 562-(1974).
17. M.L. Standaert and R.J. Pollet: Equilibrium model for insulin-induced receptor down-regulation. Regulation of insulin receptors in differentiated BC3H-1 myocytes. *J. Biol. Chem.* **259**, 2346-2354 (1984).
18. H. Sato, T. Terasaki, K. Okumura, and A. Tsuji: Effect of receptor up-regulation on insulin pharmacokinetics in streptozotocin-treated diabetic rats. *Pharm. Res.* **8**, 563-569 (1991).
19. J.W. Cox, S.R. Cox, G. VanGiessen, and M.J. Ruwart: Ibuprofen Stereoisomer hepatic clearance and distribution in normal and fatty *in situ* perfused rat liver. *J. Pharmacol. Exp. Ther.* **232**, 636-643 (1985).
20. F.G. Hamel, B.I. Posner, J.J.M. Bergeron, B.H. Frank, and W.C. Duckworth: Isolation of insulin degradation products from endosomes derived from intact rat liver. *J. Biol. Chem.* **263**, 6703-6708 (1988).
21. H. Sato, A. Tsuji, K. Hirai, and Y.S. Kang: Application of HPLC in disposition study of A14-^{125}I-labeled insulin in mice. *Diabetes* **39**, 563-569 (1990).
22. H. Sato, Y. Sugiyama, Y. Sawada, T. Iga, and M. Hanano: Binding of radioiodinated human β-endorphin to serum proteins from rats and humans, determined by several methods. *Life Sci.* **1985**, 1309-1318 (1985).
23. P. De Meytes, A.R. Bianco, and J. Roth: Site-site interactions among insulin receptors. Characterization of the negative cooperativity. *J. Biol. Chem.* **251**, 1877-1888 (1976).
24. J.R. Levy and J.M. Olefsky: The trafficking and processing of insulin and insulin receptors in cultured rat hepatocytes. *Endocrinology* **121**, 2075-2086 (1987).
25. J.W. De Pierre and M.L. Karnovsky: Plasma membranes of mammalian cells. *J. Cell. Biol.* **56**, 275-303 (1973).
26. J.J.M. Bergeron, G. Levine, R. Sikstrom, D. O'Shaughnessy, B. Kopriwa, N.J. Nadler, and B.I. Posner: Polypeptide hormone binding sites *in vivo*: initial localization of ^{125}I-labeled

insulin to hepatocyte plasmalemma as visualized by electron microscope radioautography. *Proc. Natl. Acad. Sci. USA* **74**, 5051-5055 (1977).

27. J.J.M. Bergeron, R. Sikstrom, A.R. Hand, and B.I. Posner: Binding and uptake of ^{125}I-insulin into rat liver hepatocytes and endothelium. An in vivo radioautographic study. *J. Cell. Biol.* **80**, 427-443 (1979).
28. F.G. Williams, D.E. Johnson, and G.E. Bauer: [^{125}I]-Insulin metabolism by the rat liver in vivo: evidence that a neutral thiol-protease mediate rapid intracellular insulin degradation. *Metabolism* **39**, 231-241 (1990).
29. D.B. Donner: Receptor- and non-receptor-mediated uptake and degradation of insulin by hepatocytes. *Biochem J.* **208**, 211-219 (1982).
30. P.O. Seglen: Preparation of rat liver cells. III. Enzyme requirements for tissue dispersion. *Exp. Cell Res.* **82**, 391-398 (1973).
31. S. Gammeltoft, LØ. Kristensen, and L. Sestoft: Insulin receptors in isolated rat hepatocytes. *J. Biol. Chem.* **253**, 8406-8413 (1978).
32. H.J.L. Frank, M.B. Davidson, and P.A. Serbin: Insulin binding and action in isolated rat hepatocytes: evidence for spare receptors. *Metabolism* **30**, 1159-1164 (1981).
33. W.F. Ward and A.L. Moss: Effects of lysosomal inhibitors on ^{125}I-insulin and ^{125}I-asialofetuin degradation by the isolated, perfused rat liver and isolated rat hepatocytes. *Diabetes* **34**, 446-451 (1985).

34. R.H. Jones, P.H. Sönksen, M.A. Boroujerdi, and E.R. Carson: Number and affinity of insulin receptors in intact human subjects. *Diabetologia* **27**, 207-211 (1984).
35. R.P. Eaton, R.C. Allen, and D.S. Schade: Hepatic removal of insulin in normal man: dose reponse to endogenous insulin secretion. *J. Clin. Endocrinol. Metab.* **56**, 1294-1300 (1983).
36. A. Tsuji, T. Yoshikawa, K. Nishide, H. Minami, M. Kimura, E. Nakashima, T. Terasaki, E. Miyamoto, C.H. Nightingale, and T. Yamana: Physiologically based pharmacokinetic model for β-lactam antibiotics I: tissue distribution and elimination in rats. *J. Pharm. Sci.* **72**, 1239-1252 (1983).
37. H. Sato, Y. Sugiyama, Y. Sawada, T. Iga, and M. Hanano: Physiologically based pharmacokinetics of radioiodinated human β-endorphin in rats. An application of the capillary membrane-limited model. *Drug Metab. Dispos.* **15**, 540-550 (1987).
38. S. Terris and D.F. Steiner: Binding and degradation of ^{125}I-insulin by rat hepatocytes. *J. Biol. Chem.* **250**, 8389-8398 (1975).
39. C.A. Surmacz, J.J. Wert, Jr., W.F. Ward, and G.E. Mortimore: Uptake and intracellular fate of [^{14}C]sucrose-insulin in perfused rat livers. *Am. J. Physiol.* **255**, C70-C75 (1988).

Table 1.

Characteristics of the perfused mouse liver[a]

Characteristics	Value
Body weight (g)	31.26 ± 0.49 (10)
Liver weight (g)	1.43 ± 0.04 (10)
Endogenous insulin	N.D.[b] (10)
Perfusion pressure (mmHg)	15-18
GOT releasing rate constant (min^{-1})	0.0108 ± 0.0095[c] (4)
GPT releasing rate constant (min^{-1})	0.0112 ± 0.0102[c] (4)
CL_H ($ml \cdot min^{-1}$ per liver)[d]	
Low dose (0.018 nmol/l)	0.89
High dose (2.0 nmol/l)	0.52
$CL_{int,app}$ ($ml \cdot min^{-1}$ per g liver)[e]	
Low dose (0.018 nmol/l)	1.33
High dose (2.0 nmol/l)	0.53

[a] Numbers in parentheses indicate the number of perfused liver preparations from mice;

[b] Not detected by radioimmunoassay (< 100 pmol/l);

[c] Expressed as the mean ± SEM, as assessed by a linear least-squares regression of the GOT and GPT activity (milliunits per milliliter) *vs.* time curves;

[d] Determined by Eq.9, using the perfusate volume (V_p) and exponential slope (k_e) of the disappearance of A_{14}-^{125}I-insulin from the reservoir perfusate;

[e] Determined by Eq.10, using the f_p (= 1.0), $CL_{int,app}$ and Q_p values.

Table 2.

Parameters used in model prediction of hepatic elimination and distribution of insulin in the perfused mouse liver

Parameters	Symbol	Value	Units	Source
Extracellular volume	V_e	0.55	ml	experiment[a]
Perfusate volume	V_p	12.0	ml	experiment
Perfusion flow rate (without erythrocytes)	Q_p	1.67	$ml \cdot min^{-1}$	experiment
Fraction unbound to proteins	f_p	1.0		experiment
Insulin-receptor association rate constant	k_{on}	2.4×10^8	$min^{-1} \cdot mol^{-1} \cdot l$	ref. 31
Insulin-receptor dissociation rate constant	k_{off}	0.12	min^{-1}	ref. 31
Receptor total number	R_T	8.66 ± 0.48	pmol per g liver	estimation[b]
Endocytotic rate constant of occupied receptor	k_{end}	0.62 ± 0.03	min^{-1}	estimation[b]
Endocytotic rate constant of unoccupied receptor	k_{sp}	0.022 ± 0.010	min^{-1}	calculation[c]
Receptor returning rate constant	k_{ret}	0.11 ± 0.02	min^{-1}	calculation[d]
Intracellular degradation rate constant	k_{deg}	0.907 ± 0.057	min^{-1}	estimation[b]

[a] Obtained as the sum of interstitial volume (V_{IS}) and capillary volume (V_{CB}). The V_{IS} was determined to be 0.55 ml using ^{14}C-inulin in mice (unpublished observation), and the V_{CB} was extrapolated from the reference value in the rat liver [36] to be 0.14 ml in the mouse liver;

[b] Mean ± SD, estimated from the observed data on X_s, X_i, X_{deg} and C_p (Fig. 6) according to Eqs.1-6 and 8, using a nonlinear least-squares regression analysis [16];

[c] Mean ± SD, estimated from the reported data [11] according to Eq.11 using a nonlinear least-squares regression analysis [16];

[d] Mean ± SD, estimated from the reported data [10] according to Eq.19 using a nonlinear least-squares regression analysis [16].

FIGURE LEGENDS

Fig. 1. *The receptor-recycling model of hepatic insulin clearance and distribution.*

Solid and broken arrows indicate the movements of insulin and its receptors, respectively. The liver is subdivided into the three compartments, i.e., extracellular fluid, cell surface and intracellular (vesicular) space, which are assumed to be well-mixed. Since the partition of A_{14}-^{125}I-insulin to erythrocytes could be neglected by the method described previously [37], the erythrocyte compartment is not considered. R_s and R_i defines the numbers of surface and internalized receptors, respectively. X_b, X_i and X_{deg} define the amounts of surface-bound insulin, internalized insulin and the intracellular degradation products of insulin, respectively. C_p and C_e define the concentrations in the perfusate and extracellular fluid, respectively. The rate constant k_{rel} defines the release of X_{deg} into the extracellular fluid. The other nomenclature is presented in Table 2. Receptor synthesis, processing and degradation are not involved in this model, because the half-time of receptor turnover, 10 hr [8], far exceeds the time interval (30 min) of the present liver perfusion. The nonspecific binding of insulin to hepatocytes was neglected, because it is only about 8% of the total binding in isolated rat hepatocytes [38]. Since very little ^{14}C-sucrose is taken up by perfused rat livers [39], this model confine itself to receptor-mediated endocytosis over and above fluid-phase endocytosis. The total number of mobile receptors, R_T ($= R_s + R_i$), and receptor affinity, K_d ($= k_{off}/k_{on}$), are assumed to be constant throughout the experiment, according to the previous reports [9,10].

Fig. 2. *HPLC profiles of A_{14}-^{125}I-insulin in the perfusate after 0 min (A), 10 min (B), 15 min (C), 20 min (D) and 30 min (E) perfusion of the mouse livers.*

Open circles represent ^{125}I-radioactivity (cpm) in 0.8-ml fractions eluting from μ-Bondapak C_{18} column (30 cm x 3.9 mm i.d., Waters), which had been standardized with 3-I-L-tyrosine, A_{14}-^{125}I-insulin and unlabeled porcine insulin, with the acetonitrile gradient shown by a broken line. Flow rate was set at 1.0 ml·min^{-1}.

Fig. 3. *Relationship of percentage of intact A_{14}-^{125}I-insulin between trichloroacetic acid (TCA)-precipitation and high-performance liquid chromatography (HPLC) methods in perfusates obtained 0 (●), 10 (○), 15 (■), 20 (□), 30 (▲) and 45 (△) min after the administration of A_{14}-^{125}I-insulin into the reservoir of cyclically perfused mouse liver.*

The percentage of radioactivity precipitable by TCA was calculated as (cpm in precipitate)/[(cpm in precipitate) + (cpm in supernatant)] x 100, whereas the percentage of intact A_{14}-^{125}I-insulin on HPLC was calculated by comparing the peak areas of radioactivity eluted from the column.

Fig. 4. *The disappearance of A_{14}-^{125}I-insulin from the perfusate (○) and the appearance of its degradation products in the perfusate (●), after bolus administration of a tracer amount of A_{14}-^{125}I-insulin into the reservoir (0.018 nmol/l in a final concentration) in the perfused mouse liver.*

Each point and vertical bar represent the mean ± SEM from 3-13 rats

(for labeled insulin) or 4 rats (for degradation products). When A_{14}-^{125}I-insulin was perfused in the perfusion apparatus without the liver, no loss of the ^{125}I-radioactivity from the reservoir was observed. Thus, the disappearance of A_{14}-^{125}I-insulin from the reservoir was not due to adsorption of labeled peptide to the perfusion apparatus, but to hepatic elimination. Moreover, when portions of perfusate were occasionally obtained from the perfused livers to examine *in vitro* degradation of A_{14}-^{125}I-insulinat 37°C, there was essentially no change in insulin concentration for up to 60 min. Therefore, the release of proteases from the perfused livers was negligible.

Fig. 5. *A representative elution profile of ^{125}I-radioactivity through the outflow cannula during 5-min wash with saline and 20-min wash with acidic buffer (pH 3.5) at 4°C, after A_{14}-^{125}I-insulin was perfused for 30 min in a cyclically perfused mouse liver.*

Briefly, the livers were replaced in an open-circuit system and washed for 5 min with ice-cold saline at the flow rate of 2.5 ml·min^{-1}, to remove unbound ^{125}I-radioactivity in the extracellular fluid and within the cannula. The livers were then perfused for 20 min with acidic buffer (acetic acid 100 mmol/l; mannitol 100 mmol/l; NaCl 45 mmol/l; pH 3.5) at the flow rate of 2.5 ml·min^{-1}.

Fig. 6. *The clearance of A_{14}-^{125}I-insulin by cyclically perfused mouse livers at low (0.018 nmol/l; ●) and high (2 nmol/l; ○) doses (in panel A).*

The perfusate concentrations of A_{14}-^{125}I-insulin at a low dose in Fig. 4 are presented again in a logarithmic plot. Each point and bar

represent the mean ± SEM from 3-13 rats (for a low dose) or 4 rats (for a high dose). In panel B, the time-courses of acid-extractable (○) and acid-resistant (●) A_{14}-^{125}I-insulin, as well as that of acid-resistant degradation products (▲) of A_{14}-^{125}I-insulin are presented. Each point and vertical bar represent the mean ± SEM from 4 rats. In panels A and B, solid and dashed lines show the computer-generated simulation curves using "receptor-recycling" ($k_{ret} \neq 0$) and "non-receptor-recycling" ($k_{ret} = 0$) models of hepatic insulin clearance. Especially, the curves indicated by arrows provide prediction of the disappearance of A_{14}-^{125}I-insulin at a high dose (2 nmol/l), using the set of parameters determined at the low dose (0.018 nmol/l).

Fig. 7. *Computer simulation of the time-dependent changes in the perfusate concentration of A_{14}-^{125}I-insulin (panel A) and surface receptor number (panel B) at varying initial concentrations of insulin in the reservoir, using the "receptor-recycling" model of hepatic insulin clearance and distribution.*

Fig. 1

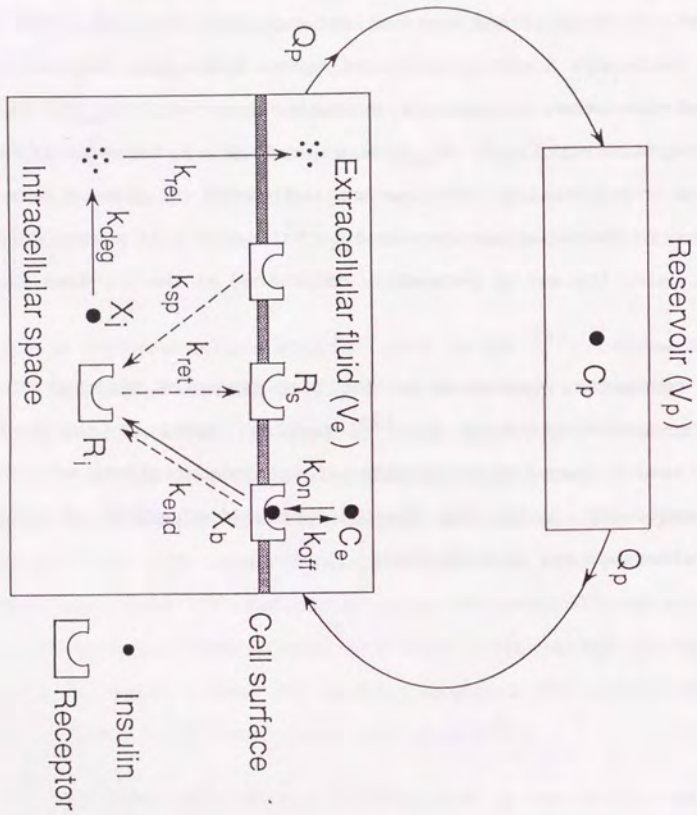
Qp
Reservoir (Vp)
Cp
Qp
Extracellular fluid (Ve)
Intracellular space
Cell surface
Ce
kon
koff
Rs
Ri
Xb
Xi
krel
ksp
kret
kdeg
kend
Insulin
Receptor

Fig. 2

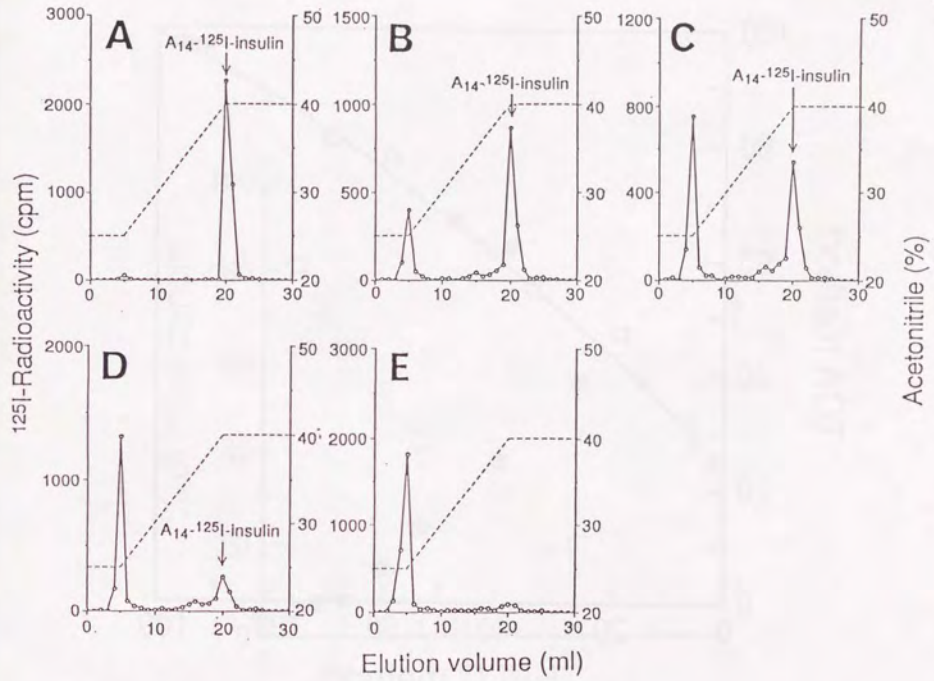
A
B
C
D
E
A14-125I-insulin
125I-Radioactivity (cpm)
Acetonitrile (%)
Elution volume (ml)

Fig. 3

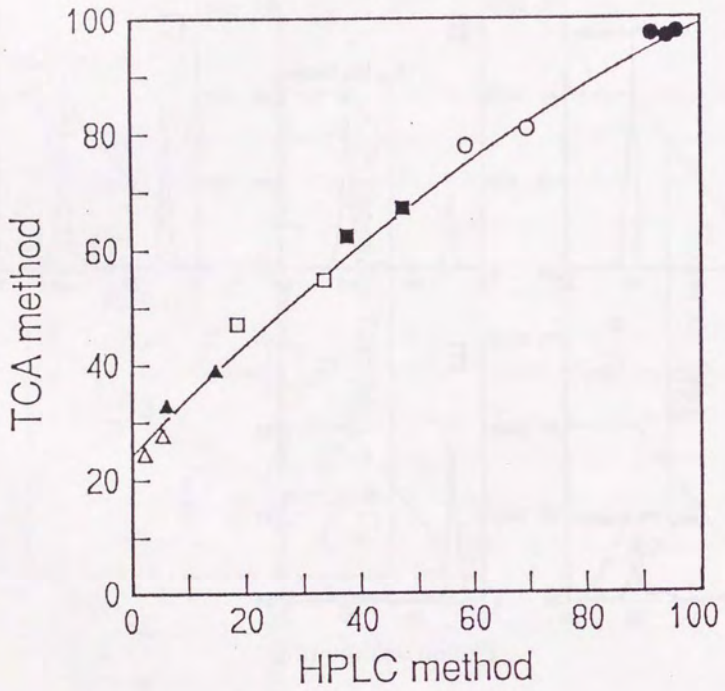
TCA method
HPLC method
0
20
40
60
80
100

Fig. 4

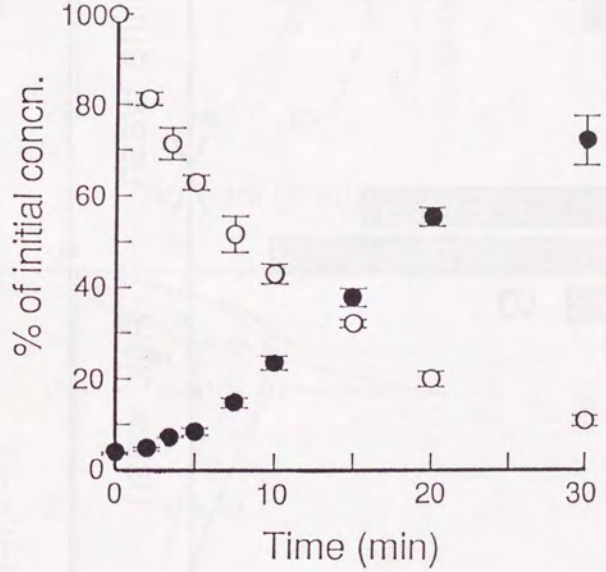
% of initial concn.
Time (min)
0
20
40
60
80
100
0
10
20
30

Fig. 6

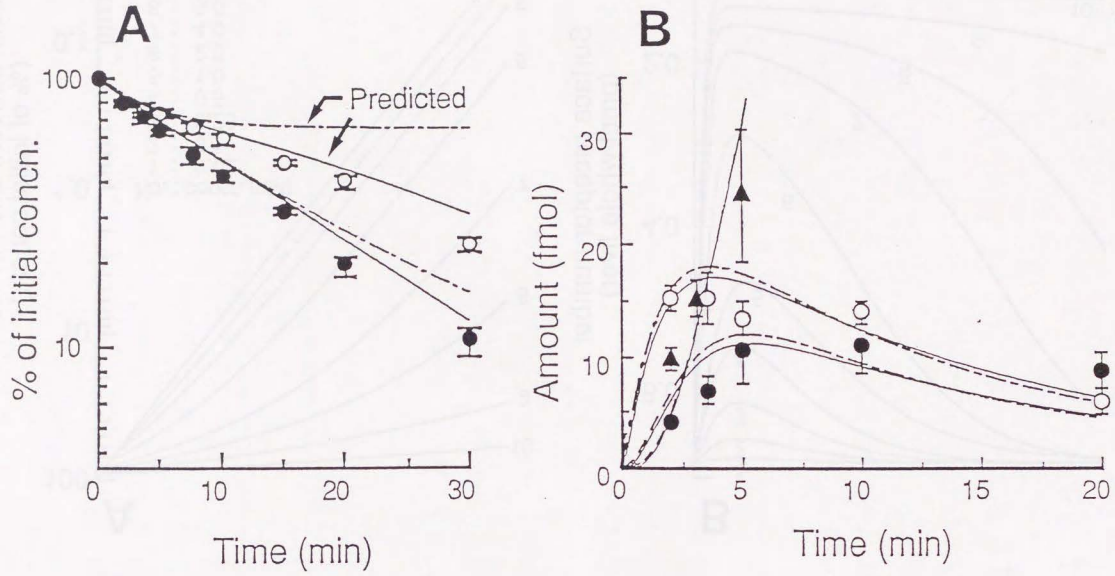
A
100
10
% of initial concn.
Predicted
0
10
20
30
Time (min)
B
30
20
10
0
Amount (fmol)
0
5
10
15
20
Time (min)

Fig. 5

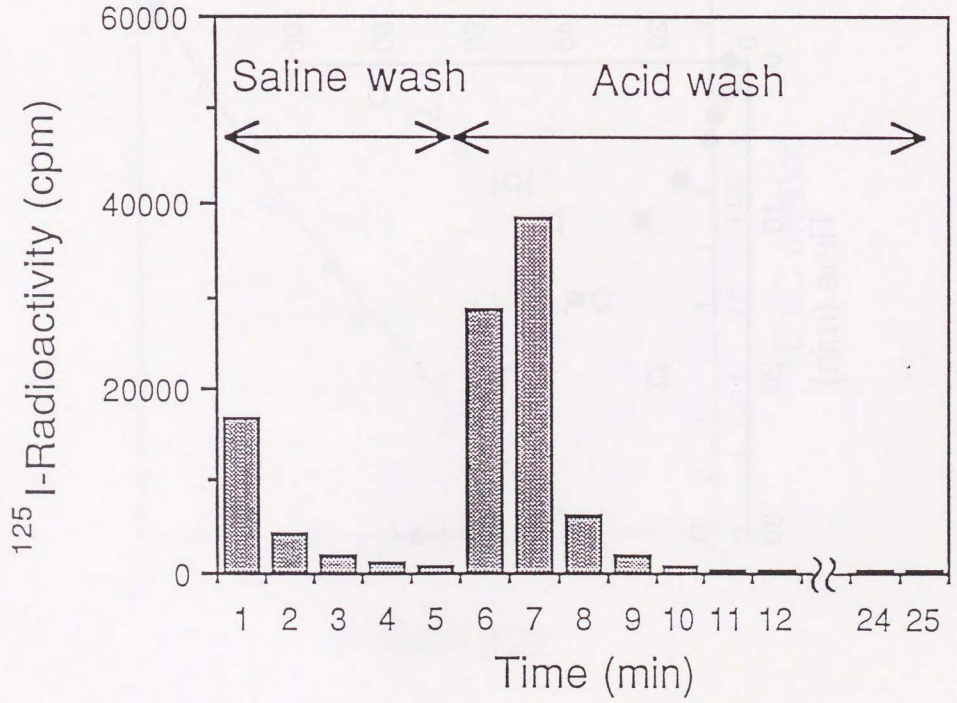
60000
40000
20000
0
125I-Radioactivity (cpm)
Saline wash
Acid wash
1 2 3 4 5 6 7 8 9 10 11 12 24 25
Time (min)

Fig. 7

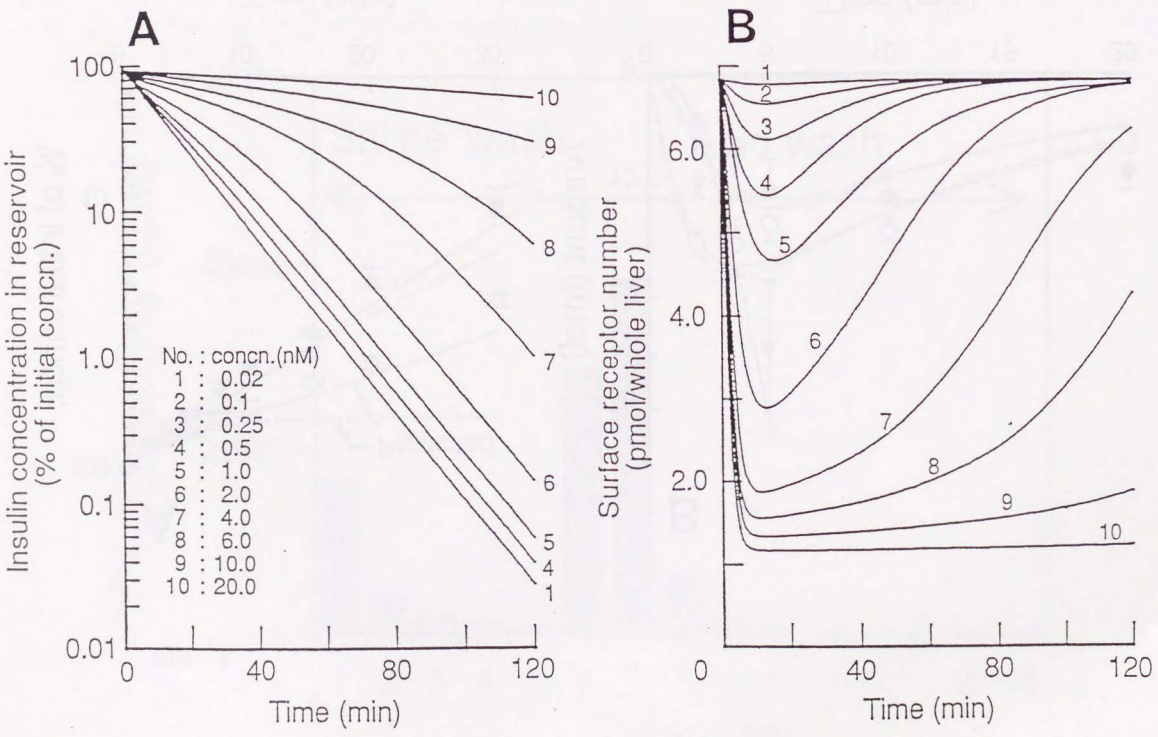
A
B
Insulin concentration in reservoir
(% of initial concn.)
100
10
1.0
0.1
0.01
No. : concn.(nM)
1 : 0.02
2 : 0.1
3 : 0.25
4 : 0.5
5 : 1.0
6 : 2.0
7 : 4.0
8 : 6.0
9 : 10.0
10 : 20.0
0
40
80
120
Time (min)
Surface receptor number
(pmol/whole liver)
6.0
4.0
2.0
0
Time (min)

PART X

PHYSIOLOGICAL MODELING OF RECEPTOR-MEDIATED DISTRIBUTION AND ELIMINATION OF INSULIN IN MICE

SUMMARY

In order to predict the distribution and elimination of insulin in mice, we proposed a physiological model incorporating the receptor binding, receptor-mediated endocytosis, intracellular degradation of insulin, and receptor recycling in the liver, as well as transcapillary diffusion and receptor binding in the extrahepatic tissues. The vascular permeability clearances of ^{14}C-inulin in various tissues in mice were estimated from the observed data using a hybrid model analysis, and assumed to be equal to those of A_{14}-^{125}I-insulin. A simple method of estimating the *in vivo* receptor binding capacity (R_S), which overcomes the effect of slow vascular permeability of insulin, was developed and showed that specific binding sites of insulin exist in various tissues and the rank order of surface receptor density was liver > kidney > lung ≑ spleen ≑ gut > heart >> muscle ≑ adipose >> brain. Numerically and simultaneously solving the differential equations describing the model as to plasma and various tissues, predicted concentration curves of A_{14}-^{125}I-insulin corresponded well with the observed data at low (tracer) and high (8 U/kg) doses in mice, indicating the feasibility of our model. Moreover, since this model incorporates the recycling of receptors as the cellular mechanism of hepatic insulin clearance, *in vivo* down-regulation could be predicted in relation to insulin concentration in the ISF. The methods and principles developed here can be applied to other biologically active peptides and proteins, with adequate modifications of the model.

INTRODUCTION

Recently, we have demonstrated the important roles of receptor binding in the distribution and elimination of insulin *in vivo* (1,2), and quantitatively analyzed the receptor-mediated endocytosis (RME)[1] of insulin in perfused kidneys (3) and livers (4), by applying an acid-wash technique (5) to distinguish between the surface-bound and internalized insulin in an intact organ. In these kinetic studies (1-4), receptor-mediated saturable processes were clearly resolved by the use of a biologically active radiolabeled insulin with a high specific activity, A_{14}-^{125}I-insulin (6), and by the use of a high-performance liquid chromatography (HPLC) to separately measure intact insulin and its immunoreactive, insulin-sized intermediate products.

Concerning the pharmacokinetic analysis of insulin, a few authors (7,8) have included receptor compartments into conventional compartmental models, in which receptor-bound insulin is subject to further degradation. Despite its potential clinical utility, however, a compartmental model cannot predict the time course of drug concentration in any target tissue, since it lacks anatomical and physiological reality in nature. On the other hand, by incorporating certain known or hypothetical mechanisms underlying the cellular distribution, uptake, and metabolism of a given drug in a physiological context, a physiological model can comprehensively predict drug concentrations in any anatomical regions of interest, including practically inaccessible biological fluids and specific sites of tissues.

Therefore, one of the authors (H.S.) has successfully described a relatively slow distribution of an opioid peptide, ^{125}I-β-endorphin, after intravenous (iv) injection to rats (9), by applying our

preliminarily proposed capillary-limited physiological model which includes vascular permeability clearances (10,11). However, receptor binding of the peptide was not explicitly incorporated in the previous physiological model (9), while the receptor-mediated distribution and degradataion of opioid peptides have been suggested by separate experiments (12-15). On the other hand, we have developed an organ model of hepatic insulin distribution and clearance, which includes the cellular events of receptor binding, RME (16,17), and receptor recycling (18,19), namely a "receptor-recycling" model (4). Since the liver plays a major role in the receptor-mediated clearance of insulin (20) and exogenously administered insulin is significantly distributed to its receptors in various tissues (21), we came to incorporate the receptor-recycling model into the capillary-limited physiological model. Unique to this model is the ability to predict the changes in surface receptor number (e.g., down-regulation) in relation to plasma insulin concentrations at a given dose. Using this physiological model, we attempted to predict the distribution and elimination of insulin at low and high iv doses in mice.

MATERIALS AND METHODS

Experimental Design and Methods. A_{14}-^{125}I-insulin or ^{14}C-inulin was intravenously injected to mice, and tracer concentrations in plasma and tissues were determined by a trichloroacetic acid (TCA) precipitation and HPLC analysis for labeled insulin, or by an oxidation method for labeled inulin. Details concerning the animals, chemicals, experimental design, and analytical methods have been described in a previous report from our laboratory (1). The doses of insulin used were 3.25 pmol/kg (6.5 μCi/kg) and 57.4 nmol/kg (8 U/kg), which are designated as low and high doses, respectively.

Plasma Protein Binding. The binding of A_{14}-^{125}I-insulin to plasma proteins was examined according to a polyethylene glycol (PEG) precipitation method described previously (22).

Development of Organ Models. Each tissue is subdivided anatomically into three compartments, i.e., the capillary bed, the interstitial fluid (ISF), and the intracellular (vesicular) space, which are assumed to be well-stirred. Since our preliminary experiment using the method described previously (9) showed that the partition of A_{14}-^{125}I-insulin to mouse erythrocytes is negligible, an erythrocyte compartment was not included in the model. It is assumed that only insulin unbound to plasma proteins is subject to transcapillary exchange, receptor binding, and glomerular filtration. The disposition of A_{14}-^{125}I-insulin in various tissues are modeled in details as follows (for abbreviations and symbols, see Appendix I):

Liver. The "receptor-recycling model" (Model A in fig. 1), developed recently (4), was applied to the liver. Several assumptions, approximations, and limitations of this model have been described in the previous study (4). The differential equations

describing the system are given as follows:

$$V_{CB}\frac{dC_{CB}}{dt} = \begin{pmatrix}\text{rate of}\\ \text{entry by}\\ \text{plasma flow}\end{pmatrix} - \begin{pmatrix}\text{rate of}\\ \text{exit by}\\ \text{plasma flow}\end{pmatrix} - \begin{pmatrix}\text{net rate of}\\ \text{transcapillary}\\ \text{exchange}\end{pmatrix} \quad (1)$$

$$V_{IS}\frac{dC_{IS}}{dt} = \begin{pmatrix}\text{net rate of}\\ \text{transcapillary}\\ \text{exchange}\end{pmatrix} - k_{on}\cdot f_{IS}\cdot C_{IS}(R_s - X_s) + k_{off}\cdot X_s \quad (2)$$

$$\frac{dX_s}{dt} = k_{on}\cdot f_{IS}\cdot C_{IS}(R_s - X_s) - (k_{off} + k_{end})X_s \quad (3)$$

$$\frac{dX_i}{dt} = k_{end}\cdot X_s - k_{deg}\cdot X_i \quad (4)$$

$$\frac{dR_s}{dt} = k_{ret}\cdot R_i - k_{end}\cdot X_s - k_{sp}(R_s - X_s) \quad (5)$$

$$\frac{dR_i}{dt} = k_{end}\cdot X_s + k_{sp}(R_s - X_s) - k_{ret}\cdot R_i \quad (6)$$

The anatomy of the liver (23) allows a rapid equilibrium of insulin between the capillary bed and ISF (i.e., Disse Space). Thus, summation of eqs. 1 and 2, and rearrangement using the equilibrium condition of $f_p\cdot C_{CB} = f_{IS}\cdot C_{IS}$ gives:

$$(f_{IS}\cdot V_{CB}/f_p + V_{IS})\frac{dC_{IS}}{dt} = \begin{pmatrix}\text{rate of}\\ \text{entry by}\\ \text{plasma flow}\end{pmatrix} - \begin{pmatrix}\text{rate of}\\ \text{exit by}\\ \text{plasma flow}\end{pmatrix} - k_{on}\cdot f_{IS}\cdot C_{IS}(R_s - X_s) + k_{off}\cdot X_s \quad (7)$$

Since f_{IS} is defined as the ratio of $C_{IS,u}/(C_{IS,u} + C_{IS,b})$, and $C_{IS,b}$ represents the nonspecifically bound A_{14}-^{125}I-insulin in the ISF, f_{IS} can be expressed as follows, using a nonspecific binding constant, α:

$$f_{IS} = \frac{1}{1 + \alpha} \quad (8)$$

Since the changes in R_s and R_i are determined not only by exogenous insulin, but also by endogenous insulin in the portal vein (C^*_{pv}), the

differential mass-balance equations of endogenous insulin (i.e., C^*_{IS}, X^*_s and X^*_i) were simultaneously solved with those of labeled insulin at the basal level of portal insulin measured at the time of experiments. The initial values of R_s and R_i were obtained from the simulation of a single-pass perfused liver system at steady state.

Kidney. We propose Model B (fig. 1) for the renal handling of insulin. The differential equations describing this system are essentially the same as used in a previous study (9), except for the presence of specific receptors in the ISF (for a complete set of equations, see Appendix III).

Other Tissues. We propose Model C (fig. 1) for noneliminating tissues except for the spleen and brain. This model includes vascular permeability between the capillary bed and ISF, equilibrium receptor binding and nonspecific binding in the ISF. Thus, the differential equations describing C_{CB} and C_{IS} are given as follows, respectively:

$$V_{CB}\frac{dC_{CB}}{dt} = Q_p(C_p - C_{CB}) - P(f_p\cdot C_{CB} - f_{IS}\cdot C_{IS}) \quad (9)$$

$$V_{IS}\frac{dC_{IS}}{dt} = P(f_p\cdot C_{CB} - f_{IS}\cdot C_{IS}) \quad (10)$$

where C_{IS} defined here is not the actual concentration of insulin in the ISF as defined in Model A, but represents the functional or apparent concentration of insulin in the ISF including cell surface compartment. Thus, C_{IS} can be described as follows, using the nonspecific binding constant (α) and surface receptor number (R_s) in the ISF:

$$C_{IS} = C_{IS,u} + C_{IS,b} + X_s/V_{IS} = C_{IS,u} + \alpha\cdot C_{IS,u} + \frac{(R_s/V_{IS})C_{IS,u}}{K_d + C^*_{IS,u} + C_{IS,u}} \quad (11)$$

where $C^*_{IS,u}$ represents the endogenous insulin concentration in the ISF. Therefore, f_{IS} can be expressed as follows:

$$f_{IS} = \frac{C_{IS,u}}{C_{IS}} = \frac{1}{1 + \alpha + \frac{R_s/V_{IS}}{K_d + C^*_{IS,u} + C_{IS,u}}} \quad (12)$$

On the other hand, the C_{IS} is also expressed as follows:

$$C_{IS} = V_T/V_{IS}\ C_T \quad (13)$$

Substituting C_{IS} in eqs. 9 and 10 according to eq. 13 gives:

$$V_{CB}\frac{dC_{CB}}{dt} = Q_p(C_p - C_{CB}) - P(f_p \cdot C_{CB} - f_{IS} \cdot V_T/V_{IS} \cdot C_T) \quad (14)$$

$$V_T\frac{dC_T}{dt} = P(f_p \cdot C_{CB} - f_{IS} \cdot V_T/V_{IS} \cdot C_T) \quad (15)$$

The tissue-to-plasma concentration ratio (K_p) is defined as:

$$K_p = C_{T,ss}/C_{CB,ss} = V_{IS}/V_T \cdot C_{IS,ss}/C_{CB,ss} \quad (16)$$

where $C_{T,ss}$ and $C_{CB,ss}$ represent the steady state concentrations in the capillary bed and ISF, respectively. At steady state, unbound insulin concentrations in the capillary bed and ISF are equivalent, because an active transport of the peptide across the capillary wall is not assumed. Thus, the following relationship between $C_{CB,ss}$ and $C_{IS,ss}$ holds:

$$f_p \cdot C_{CB,ss} = f_{IS} \cdot C_{IS,ss} \quad (17)$$

According to eqs. 16 and 17, f_{IS} can be expressed as follows:

$$f_{IS} = f_p \cdot V_{IS}/V_T/K_p \quad (18)$$

According to eq. 18, eqs. 14 and 15 can be further written as:

$$V_{CB}\frac{dC_{CB}}{dt} = Q_p(C_p - C_{CB}) - P \cdot f_p(C_{CB} - C_T/K_p) \quad (19)$$

$$V_T\frac{dC_T}{dt} = P \cdot f_p(C_{CB} - C_T/K_p) \quad (20)$$

For the spleen, we propose Model D (fig. 1) which includes a rapid equilibrium of insulin between the capillary bed and ISF, as well as equilibrium receptor binding and nonspecific binding in the ISF. Therefore, summation of eqs. 19 and 20, and rearrangement using the relationship $C_{CB} = K_p/f_p \cdot V_T/V_{IS} \cdot C_T$ gives:

$$(V_{CB}/K_p + V_T)\frac{dC_T}{dt} = Q_p(C_p - C_T/K_p) \quad (21)$$

For the brain, we propose Model E (fig. 1) which includes the equilibrium surface receptor binding and nonspecific binding of insulin in the capillary bed. Thus, the changes in C_{CB} can be described as:

$$V_{CB}\frac{dC_{CB}}{dt} = Q_p(C_p - C_{CB}) \quad (22)$$

Rearrangement of eq. 22 according to the definition of $K_p = C_T/C_{CB}$ gives:

$$(V_{CB}/K_p)\frac{dC_T}{dt} = Q_p(C_p - C_T/K_p) \quad (23)$$

Data Analysis. The V_{IS} of each tissue was determined as:

$$V_{IS} = V_T \cdot K_{p,inu} \quad (24)$$

where $K_{p,inu}$ was determined from an apparent tissue-to-plasma concentration ratio of inulin ($K_{p,app,inu}$), at the terminal phase using the method of Chen and Gross (24). The P of ^{14}C-inulin was estimated from a hybrid model analysis (25) using a nonlinear least-squares regression analysis, NONLIN74 (26). In each tissue, the P of

A_{14}-^{125}I-insulin was assumed to be equivalent to that of ^{14}C-inulin. For noneliminating tissues, K_p (or $K_{p,ns}$) of A_{14}-^{125}I-insulin was corrected from $K_{p,app}$ (or $K_{p,app,ns}$) and P, using equations derived previously in the case of capillary-limited distribution (9), and f_{IS} (or $f_{IS,ns}$) was given by eq. 18. In the case of brain, K_p was calculated using the following equation derived from eq. 23:

$$K_p = (1 - \lambda_z \cdot V_{CB}/Q_p)K_{p,app} \quad (25)$$

where λ_z represents an exponential slope of the terminal phase. Subsequently, α and the receptor density (R_s/V_T) were calculated using eqs. A2 and A3 (eqs. A5 and A6 for the brain) in Appendix II, respectively. For the liver, α was obtained from the observed data at a high dose by the same method as mentioned above, while R_s/V_T is not necessarily constant but may change with time, as formulated in eq. 5. For the kidney, f_{IS}, $f_{IS,ns}$, and k_{seq} were simultaneously estimated by a fitting procedure.

Physiological Model. A physiological model of A_{14}-^{125}I-insulin in mice is illustrated in fig. 2, while that of ^{14}C-inulin in mice is the same as that previously used in rats (10) and rabbits (11). The physiological constants used are listed in table 1. Concerning the assignment of organ clearances for insulin, CL_H was predicted by the present and previous physiological models (4) at a given dose, while CL_R was attributed to the product of f_p and glomerular filtration rate (GFR), according to the previous result obtained using perfused rat kidneys (3). Moreover, the sum of unspecified clearances was attributed to the arterial plasma compartment as a dose-independent plasma clearance (CL_p), as follows:

$$CL_p = CL_{tot,ns} - f_p \cdot GFR \quad (26)$$

where the $CL_{tot,ns}$ represents the nonspecific total clearance, i.e., the CL_{tot} obtained at a high dose.

For both insulin and inulin, the simultaneous differential equations for all compartments in their physiological models were solved numerically by the Runge-Kutta-Gill method at a suitable interval (0.005 min) on a digital computer (FACOM-M360AP) at the Information Processing Center, Kanazawa University. The observed and predicted concentrations of the injected tracers in plasma and tissues were expressed as percentage of the dose injected per ml sample.

RESULTS

Physiological Model of ^{14}C-inulin. The calculated K_p and P values of ^{14}C-inulin in mice are listed in table 1, together with physiological parameters and constants for a 35-g mouse. The model-predicted curves of ^{14}C-inulin concentrations in plasma and various tissues are presented in fig. 3, and were shown to be in good agreement with the observed data.

Plasma Protein Binding of A_{14}-^{125}I-insulin. The fraction of A_{14}-^{125}I-insulin unbound in mouse plasma (f_p) was determined to be 0.871 $\pm$ 0.002 (mean $\pm$ SEM; n = 5) by a PEG precipitation method. Using this f_p value in eq. 26, the CL_p was calculated to be 6.66 ml/min/kg, since GFR and $CL_{tot,ns}$ were determined previously to be 11.3 ml/min/kg and 16.5 ml/min/kg (1), respectively, in mice.

Physiological Model of A_{14}-^{125}I-insulin. The endogenous insulin concentrations in the portal vein (C^*_{pv}) and carotid artery (C^*_p) at the time of experiments were 0.440 $\pm$ 0.052 nM (mean $\pm$ SEM; n = 5) and 0.281 $\pm$ 0.036 nM (mean $\pm$ SEM; n = 11), respectively. The basal R_s and R_i values in the liver were estimated to be 7.3 pmol and 6.0 pmol per liver for a 35-g mouse, respectively, using a single-pass perfusion model at the constant insulin concentration (0.44 nM), and used as initial values for the subsequent computer-aided prediction. The calculated values of K_p, $K_{p,ns}$, f_{IS}, $f_{IS,ns}$, α, and R_s/V_T are listed in table 1. The K_p and $K_{p,ns}$ values are greatly different with each other in the lung, heart, spleen and gut, while relatively close in the brain, skin, muscle and adipose. For the kidney, k_{seq} was estimated to be 1.0 min^{-1} by a fitting procedure. The obtained prediction curves of A_{14}-^{125}I-insulin for plasma and various tissues are presented in figs. 4 and 5 at low and high doses, respectively,

and were shown to be in good agreement with the observed data. Figures 6A-6D illustrate the time courses of the amounts of exogenously administered insulin in the ISF ($V_{IS} \cdot C_{IS}$), cell surface (bound to receptor)(X_s), and intracellular space (X_i), as well as those of the receptor numbers on the cell surface (R_s) and in the intracellular space (R_i).

DISCUSSION

To our knowledge to date, this is the first demonstration of a physiologically based pharmacokinetic modeling of insulin, of which pharmacokinetics have been performed only by two- (or three) compartmental or noncompartmental moment analysis so far. The present physiological model includes the receptor binding, internalization, intracellular degradation of insulin and recycling of receptors as the cellular mechanisms of hepatic insulin distribution and clearance, thus making it possible to predict the insulin-induced down-regulation of surface receptors in the liver, as observed *in vivo* (27,28). Such a prediction could not be possible if one considers a simple model in which a constant number of surface receptors is assumed (7,8). It is difficult and beyond the scope of this study, however, to assess an extraction of insulin across every tissue, and to discriminate the X_s and X_i under *in vivo* conditions. Thus, this model appears to limit itself in that it lacks the RME in the organ models of muscle and adipose, despite that insulin is taken up *via* RME by these isolated cells *in vitro* (29,30). However, before incorporating certain known biochemical processes into a physiological model, one has to evaluate the rate-limiting step(s) responsible for the distribution and elimination of a given drug. For example, with regard to the muscle and adipose, it is known that the capillary wall significantly disturbs the diffusion of insulin into interstitium (31,32), so that the transcapillary diffusion of insulin may be rate-limiting in its action (33). In fact, our preliminary simulation suggested that the rate-limiting step for the distribution of insulin in muscle and adipose lies for the most part in the slow vascular permeability of insulin, but for little part in the receptor binding process.

Moreover, insulin is not degraded in its endothelial passage (34,35) and its k_{end} values in the extrahepatic tissues are very small, as reported to be 0.0018 min^{-1} in the myocytes (30), 0.0027 min^{-1} in the adipocytes (36) and 0.022 min^{-1} in the perfused nonfiltering kidney (at the basolateral side of renal tubules) (3), which are far below that in the liver, ranging from 0.12 min^{-1}(37) to 0.62 min^{-1} (4). In addition, the receptor-mediated transcytosis of insulin across the blood-brain barrier (BBB) is very slow (38). Furthermore, in spite of the presence of receptors in the lung (39), the organ does not eliminate insulin (40). Taken together, we neglected the RME of insulin in the extrahepatic tissues within relatively a short time interval (30 min) employed.

We have already shown that the CL_{tot} and Vd_{ss} of A_{14}-^{125}I-insulin were significantly reduced by the simultaneous injection of unlabeled insulin (8 U/kg) in mice (1) and rats (2). In this study, the differences in CL_{tot} and Vd_{ss} between the two doses, which represent receptor-mediated clearance and distribution volume, respectively, were attributed to the dynamic RME in the liver and static receptor binding in various tissues, respectively. Moreover, the fact that the Vd_{ss} of A_{14}-^{125}I-insulin at the high dose (251 ml/kg) is slightly greater to that of ^{14}C-inulin (181 ml/kg) in mice (1) indicates that A_{14}-^{125}I-insulin distributes into the ISF even in the presence of excess unlabeled insulin, suggesting that the RME is not apparently operational in the transendothelial passage of insulin. This observation contrasts with a general idea that the endothelial receptors for insulin may function in the nonlysosomal (i.e., nondegradative), transendothelial transport of biologically intact

insulin (34,35). Although the exact reason for this discrepancy is uncertain at present, it is not always possible to directly compare the *in vitro* permeability through cultured endothelial cells with *in vivo* vascular permeability for insulin, because of possible differences in the extent of receptor expression and tightness of intercellular junction, or of the lack of basement membranes under *in vitro* conditions. Therefore, at the present time, we prefer a simple modeling of the vascular transport of insulin as a nonsaturable, first-order process, and assumed that the rate of transcapillary exchange of insulin is equal to that of inulin, due to the similarity of molecular weight. The relatively good agreement between the predicted and observed concentrations of insulin in plasma and various tissues (figs. 4 and 5) may imply that these assumptions are valid under a physiological condition.

As inspected from table 2, the α values calculated using eq. A2 for the extrarenal tissues (eq. A5 for the brain) were shown to be less than unity, indicating that the nonspecific binding of insulin in the ISF is relatively low in these tissues, while the high α value for the kidney may represent a large capacity of nonspecific retention e.g., luminal reabsorption *via* non-receptor-mediated endocytosis (41) of insulin in the kidney, which was not explicitly incorporated into Model B in fig. 1. Moreover, the R_S/V_T values calculated using eq. A3 (eq. 6 for the brain) represent the surface receptor density, and its rank order was liver > kidney > lung ≑ spleen ≑ gut > heart >> muscle ≑ adipose >> brain, which is consistent with the report of Whitcomb *et al.* (21) that the order of receptor binding density (per g wt.) was liver > spleen > gut > muscle ≑ adipose, using an *in vivo* radioreceptor assay. In this study, any receptors were not detected

in the skin, because both the K_p and $K_{p,ns}$ of A_{14}-^{125}I-insulin were less than $K_{p,inu}$ in this tissue (see tables 1 and 2).

One of the main advantages of physiological models relative to traditional compartmental models is the possibility of predicting the changes in drug concentration in practically inacessible tissues or specific sites of tissues, as well as predicting the drug-induced pharmacodynamic changes (42). Figures 6A and 6C suggest that, when compared with extracellular insulin, both the receptor-bound insulin and internalized insulin significantly contribute to *in vivo* distribution of the peptide in the liver at a low dose, while they show little contribution at a high dose. Moreover, figs. 6B and 6D predict that R_S rapidly decreased to approximately 20% of the basal state and does not increase within 30 min after iv injection at a high dose, while there was essentially no change in R_S at a low dose. Therefore, the present physiological model could successfully demonstrate an important role of receptor binding in the hepatic insulin disposition, as well as insulin-induced down-regulation.

In conclusion, we developed a physiologically based pharmacokinetic model of insulin, which incorporates receptor binding, RME, intracellular degradation of insulin, and recycling of receptors in the liver, as well as vascular permeability and equilibrium receptor binding in the extrahepatic tissues. Using this model, we could successfully predict the concentration profiles of A_{14}-^{125}I-insulin in plasma and various tissues after iv bolus injection at low and high doses in mice. The methods and principles developed here can be applied to other biologically active peptides and proteins with adequate modifications of the model.

Acknowledgments. This study was supported by a Grant-in-Aid for Scientific Research from the Ministry of Education, Science and Culture of Japan, Project Research Fund from the Graduate School of Natural Science and Technology, Kanazawa University, and grants from the Nakatomi Foundation and Takeda Science Foundation.

APPENDIX I

Glossary:

Q_p, plasma flow rate (ml/min)

P, vascular permeability clearance (ml/min)

CL_{tot}, total body clearance (ml/min)

CL_R, renal clearance (ml/min)

CL_p, dose-independent plasma clearance (ml/min)

E, extraction ratio across an organ

V, volume (ml)

Vd_{ss}, steady-state volume of distribution (ml)

R, number of receptors (pmol)

R_T, total number of receptors (pmol)

C, concentration of insulin (pmol/ml)

X, amount of insulin (pmol)

α, nonspecific binding constant in the ISF

f, unbound fraction of insulin

k_{on}, association rate constant of insulin to its receptors ($min^{-1} \cdot M^{-1}$)

k_{off}, dissociation rate constant for receptor-bound insulin (min^{-1})

k_{deg}, degradation rate constant for internalized insulin (min^{-1})

k_{end}, internalization rate constant for occupied surface receptors (min^{-1})

k_{sp}, spontaneous internalization constant for unoccupied surface receptors (min^{-1})

k_{ret}, returning rate constant for internalized receptors to the cell surface (min^{-1})

K_d, dissociation constant for receptor binding of insulin (nM)

K_p, tissue-to-plasma concentration ratio of insulin

$K_{p,inu}$, tissue-to-plasma concentration ratio of inulin

λ_z, exponential slope of the terminal phase (min^{-1})

I(t), dose input function (min^{-1})

θ, injection duration (min)

Subscripts:

CB, capillary bed	p, plasma
IS, interstitial fluid	lg, lung
T, whole tissue	br, brain
s, surface	ht, heart
i, intracellular	gt, gut
u, unbound	sp, spleen
b, bound	lv, liver
ns, nonspecific	kd, kidney
app, apparent	ms, muscle
v, venous	ad, adipose
ss, steady state	sk, skin
inu, inulin	RT, renal tubule

Superscript:

*, endogenous insulin

APPENDIX II

Method of Estimating Receptor Binding Capacity (R_s). When a tracer dose of A_{14}-^{125}I-insulin was injected, $C_{IS,u}$ is far below the sum of K_d and $C^*_{IS,u}$ in eq. 12. Moreover, since $C^*_{IS,u}$ was assumed to be equal to $C^*_{CB,u}$ or $f_p \cdot C^*_p$ in a noneliminating tissue, f_{IS} can be expressed as follows:

$$f_{IS} = \frac{1}{1 + \alpha + \dfrac{R_s/V_{IS}}{K_d + f_p \cdot C^*_p}} \tag{A1}$$

On the other hand, when a large amount of unlabeled insulin is simultaneously administered with A_{14}-^{125}I-insulin, eq. 8 can be approximately rearranged to:

$$\alpha = \frac{1}{f_{IS,ns}} - 1 \tag{A2}$$

where $f_{IS,ns}$ represents the unbound fraction of A_{14}-^{125}I-insulin in the ISF when surface receptors are almost blocked by excess unlabeled insulin. Thus, though f_{IS} changes over a $C^*_{IS,u}$ plus $C_{IS,u}$ range near K_d, it is approximately constant at a very low or high concentration range, if a constant $C^*_{IS,u}$ (i.e., steady state basal condition) is assumed. According to eqs. A1 and A2, the receptor binding capacity (pmol per g wt.), R_s/V_T, can be given by:

$$R_s/V_T = \left(\frac{1}{f_{IS}} - \frac{1}{f_{IS,ns}}\right)\frac{V_{IS}(K_d + f_p \cdot C^*_p)}{V_T} \tag{A3}$$

Moreover, for the brain, C_{CB} is related to C_T as follows:

$$V_T \cdot C_T = V_{CB} \cdot C_{CB} + \left(\alpha + \frac{R_s/V_{CB}}{K_d + C^*_{CB,u} + C_{CB,u}}\right) V_{CB} \cdot C_{CB,u}$$

$$= V_{CB} \cdot C_{CB} \cdot \{1 + f_p(\alpha + \beta)\} \tag{A4}$$

where β represents $R_s/V_{CB}/(K_d + C^*_{IS,u} + C_{IS,u})$. When a tracer dose

of insulin is injected at the steady state basal condition, β reduces to $K_d + f_p \cdot C_p^*$, as mentioned above. On the other hand, β should reduce to zero at a very high dose. Therefore, α and R_S/V_T can be given as follows, for the brain:

$$\alpha = (K_{p,ns}\ V_T/V_{CB} - 1)/f_p \tag{A5}$$

$$R_S/V_T = (K_p - K_{p,ns})\ \frac{K_d + f_p \cdot C_p^*}{f_p} \tag{A6}$$

APPENDIX III

Physiological Model Equations for A_{14}-^{125}I-insulin.

Venous plasma:

$$\begin{aligned} V_v(dC_v/dt) = {} & Q_{p,br} \cdot C_{CB,br} + Q_{p,ht} \cdot C_{CB,ht} + Q_{p,ms} \cdot C_{CB,ms} \\ & + Q_{p,ad} \cdot C_{CB,ad} + Q_{p,sk} \cdot C_{CB,sk} + Q_{p,kd} \cdot C_{CB,kd} \\ & + Q_{p,lv} \cdot f_{IS,lv} \cdot C_{IS,lv}/f_p - Q_{p,lg} \cdot C_v \\ & + \text{Dose} \cdot I(t) \end{aligned} \tag{A7}$$

I(t) is the dose input function proposed by Bishoff and Dedrick (43) and expressed as:

$$I(t) = 30/\theta \cdot (t/\theta)^2 \cdot (1 - t/\theta)^2 \tag{A8}$$

where θ is the injection duration in minutes.

Lung:

$$\begin{aligned} V_{CB,lg}(dC_{CB,lg}/dt) = {} & Q_{p,lg}(C_v - C_{CB,lg}) \\ & - P_{lg} \cdot f_p(C_{CB,lg} - C_{T,lg}/K_{p,lg}) \end{aligned} \tag{A9}$$

$$V_{T,lg}(dC_{T,lg}/dt) = P_{lg} \cdot f_p(C_{CB,lg} - C_{T,lg}/K_{p,lg}) \tag{A10}$$

Arterial plasma:

$$V_p(dC_p/dt) = Q_{p,lg}(C_{CB,lg} - C_p) - C_p \cdot CL_p \tag{A11}$$

Brain:

$$(V_{CB,br}/K_{p,br})(dC_{T,br}/dt) = Q_{p,br}(C_p - C_{T,br}/K_{p,br}) \tag{A12}$$

Heart:

$$\begin{aligned} V_{CB,ht}(dC_{CB,ht}/dt) = {} & Q_{p,ht}(C_p - C_{CB,ht}) \\ & - P_{ht} \cdot f_p(C_{CB,ht} - C_{T,ht}/K_{p,ht}) \end{aligned} \tag{A13}$$

$$V_{T,ht}(dC_{T,ht}/dt) = P_{ht} \cdot f_p(C_{CB,ht} - C_{T,ht}/K_{p,ht}) \tag{A14}$$

Gut:

$$\begin{aligned} V_{CB,gt}(dC_{T,gt}/dt) = {} & Q_{p,gt}(C_p - C_{CB,gt}) \\ & - P_{gt} \cdot f_p(C_{CB,gt} - C_{T,gt}/K_p) \end{aligned} \tag{A15}$$

$$V_{T,gt}(dC_{T,gt}/dt) = P_{gt} \cdot f_p(C_{CB,gt} - C_{T,gt}/K_p) \tag{A16}$$

Spleen:

$$(V_{CB,sp}/K_{p,sp} + V_{T,sp})(dC_{T,sp}/dt) = Q_{p,sp}(C_p - C_{T,sp}/K_{p,sp}) \quad (A17)$$

Liver:

$$\begin{aligned}(f_{IS,lv}\cdot V_{CB,lv}/f_p + V_{IS,lv})(dC_{IS,lv}/dt) &= Q_{p,sp}\cdot C_{T,sp}/K_{p,sp} + Q_{p,gt}\cdot C_{CB,gt} \\ &+ (Q_{p,lv} - Q_{p,sp} - Q_{p,gt})C_p - Q_{p,lv}\cdot f_{IS,lv}\, C_{IS,lv}/f_p \\ &- k_{on}\cdot f_{IS,lv}\cdot C_{IS,lv}(R_s - X_s - X_s^*) + k_{off}\cdot X_s \quad (A18)\end{aligned}$$

$$dX_s/dt = k_{on}\cdot f_{IS,lv}\cdot C_{IS,lv}(R_s - X_s - X_s^*) - (k_{off} + k_{end})X_s \quad (A19)$$

$$dX_i/dt = k_{end}\cdot X_s - k_{deg}\cdot X_i \quad (A20)$$

$$V_{T,lv}\cdot C_{T,lv} = V_{IS,lv}\cdot C_{IS,lv} + X_s + X_i \quad (A21)$$

$$\begin{aligned}(f_{IS,lv}\cdot V_{CB,lv}/f_p + V_{IS,lv})(dC^*_{IS,lv}/dt) &= Q_{p,lv}(C^*_{pv} - f_{IS,lv}\, C^*_{IS,lv}/f_p) \\ &- k_{on}\cdot f_{IS,lv}\cdot C_{IS,lv}(R_s - X_s - X_s^*) + k_{off}\cdot X_s^* \quad (A22)\end{aligned}$$

$$dX_s^*/dt = k_{on}\cdot f_{IS,lv}\cdot C_{IS,lv}(R_s - X_s - X_s^*) - (k_{off} + k_{end})X_s^* \quad (A23)$$

$$dX_i^*/dt = k_{end}\cdot X_s^* - k_{deg}\cdot X_i^* \quad (A24)$$

$$dR_s/dt = k_{ret}\cdot R_i - k_{end}\cdot X_s - k_{sp}(R_s - X_s) \quad (A25)$$

$$dR_i/dt = k_{end}\cdot X_s + k_{sp}(R_s - X_s) - k_{ret}\cdot R_i \quad (A26)$$

Kidney:

$$\begin{aligned}V_{CB,kd}(dC_{CB,kd}/dt) &= Q_{p,kd}(C_p - C_{CB,kd}) - f_p\cdot GFR\cdot C_p \\ &- P_{kd}(f_p\cdot C_{CB,kd} - f_{IS,kd}\cdot C_{IS,kd}) \quad (A27)\end{aligned}$$

$$V_{IS,kd}(dC_{IS,kd}/dt) = P_{kd}(f_p\cdot C_{p,kd} - f_{IS,kd}\cdot C_{IS,kd}) \quad (A28)$$

$$dX_{RT}/dt = f_p\cdot GFR\cdot C_p - k_{seq}\cdot X_{RT} \quad (A29)$$

$$V_{T,kd}\cdot C_{T,kd} = V_{IS,kd}\cdot C_{IS,kd} + X_{RT} \quad (A30)$$

Muscle:

$$\begin{aligned}V_{CB,ms}(dC_{CB,ms}/dt) &= Q_{p,ms}(C_p - C_{CB,ms}) \\ &- P_{ms}\cdot f_p(C_{CB,ms} - C_{T,ms}/K_{p,ms}) \quad (A31)\end{aligned}$$

$$V_{T,ms}(dC_{T,ms}/dt) = P_{ms}\cdot f_p(C_{CB,ms} - C_{T,ms}/K_{p,ms}) \quad (A32)$$

Adipose:

$$\begin{aligned}V_{CB,ad}(dC_{CB,ad}/dt) &= Q_{p,ad}(C_p - C_{CB,ad}) \\ &- P_{ad}\cdot f_p(C_{CB,ad} - C_{T,ad}/K_{p,ad}) \quad (A33)\end{aligned}$$

$$V_{T,ad}(dC_{T,ad}/dt) = P_{ad}\cdot f_p(C_{CB,ad} - C_{T,ad}/K_{p,ad}) \quad (A34)$$

Skin:

$$\begin{aligned}V_{CB,sk}(dC_{CB,sk}/dt) &= Q_{p,sk}(C_p - C_{CB,sk}) \\ &- P_{sk}\cdot f_p(C_{CB,sk} - C_{T,sk}/K_{p,sk}) \quad (A35)\end{aligned}$$

$$V_{T,sk}(dC_{T,sk}/dt) = P_{sk}\cdot f_p(C_{CB,sk} - C_{T,sk}/K_{p,sk}) \quad (A36)$$

REFERENCES

1. H. Sato, A. Tsuji, K. Hirai, and Y.S. Kang: Application of HPLC in disposition study of A14-^{125}I-labeled insulin in mice. *Diabetes* **39**, 563-569 (1990).
2. H. Sato, T. Terasaki, K. Okumura, and A. Tsuji: Effect of receptor up-regulation on insulin pharmacokinetics in streptozotocin-treated diabetic rats. *Pharm. Res.* **8**, 563-569 (1991).
3. H. Sato, K. Yoshioka, T. Terasaki, and A. Tsuji: Receptor-mediated endocytosis of A_{14}-^{125}I-insulin by the nonfiltering perfused rat kidney. *Biochim. Biophys. Acta* **1073**, 442-450 (1991).
4. H. Sato, T. Terasaki, H. Mizuguchi, K. Okumura, and A. Tsuji: Receptor-recycling model of clearance and distribution of insulin in the perfused mouse liver. *Diabetologia*, in press.
5. T. Terasaki, K. Hirai, H. Sato, Y.S. Kang, and A. Tsuji: Absorptive-mediated endocytosis of a dynorphin-like analgesic peptide, E-2078, into the blood-brain barrier. *J. Pharmacol. Exp. Ther.* **251**, 351-357 (1989).
6. J. Gliemann, O. Sonne, S. Linde, and B. Hansen: Biological potency and binding affinity of monoiodoinsulin with iodine in tyrosine A14 or tyrosine A19. *Biochem. Biophys. Res. Com.* **87**, 1183-1190 (1979).
7. M. Berman, E.A. McGuire, J. Roth, and A.J. Zeleznik: Kinetic modeling of insulin binding to receptors and degradation in vivo in rabbits. *Diabetes* **29**, 50-59 (1980).
8. R.H. Jones, P.H. Sönksen, M.A. Boroujerdi, and E.R. Carson: Number and affinity of insulin receptors in intact human subjects. *Diabetologia* **27**, 207-211 (1984).
9. H. Sato, Y. Sugiyama, Y. Sawada, T. Iga, and M. Hanano: Physiologically based pharmacokinetics of radioiodinated human β-endorphin in rats. An application of the capillary membrane-limited model. *Drug Metab Dispos* **15**, 540-550 (1987).
10. A. Tsuji, T. Yoshikawa, K. Nishide, H. Minami, M. Kimura, E. Nakashima, T. Terasaki, E. Miyamoto, C.H. Nightingale, and T. Yamana: Physiologically based pharmacokinetic model for β-lactam antibiotics I: tissue distribution and elimination in rats. *J. Pharm. Sci.* **72**, 1239-1252 (1983).
11. A. Tsuji, K. Nishide, H. Minami, E. Nakashima, T. Terasaki, and T. Yamana: Physiologically based pharmacokinetic model for cefazolin in rabbits and its preliminary extrapolation to man. *Drug Metab. Dispos.* **13**, 729-739 (1985).
12. H. Sato, Y. Sugiyama, S. Miyauchi, Y. Sawada, T. Iga, and M. Hanano: Pharmacokinetic study of exogenously administered β-endorphin using a rapid radioreceptor assay in rats. *Life Sci.* **35**, 1051-1059 (1984).
13. H. Sato, Y. Sugiyama, S. Miyauchi, Y. Sawada, T. Iga, and M. Hanano: In vivo evidence for the specific binding of human β-endorphin to the lung and liver of the rat. *Biochem. Pharmacol.* **37**, 2273-2278 (1988).
14. H. Sato, T. Terasaki, and A. Tsuji: Specific binding and clearance of [^{3}H]dynorphin(1-13) in the perfused rat lung: an application of the multiple-indicator dilution method. *J. Pharm. Pharmacol.* **42**, 879-882 (1990).
15. H. Sato, K. Takeda, T. Terasaki, and A. Tsuji: Specific binding of β-endorphin to the isolated renal basolateral membranes in vitro. *Chem. Pharm. Bull.* **38**, 3395-3399 (1990).

16. T. Wileman, C. Harding, and P. Stahl: Receptor-mediated endocytosis. *Biochem. J.* 232, 1-14 (1985).

17. O. Sonne: Receptor-mediated endocytosis and degradation of insulin. *Physiol. Rev.* 68, 1129-1196 (1988).

18. M. Fehlman, J.L. Carpentier, E.V. Obberghen, P. Freychet, P. Thamm, D. Saunders, D. Brandenburg, and L. Orci: Internalized insulin receptors are recycled to the cell surface in rat hepatocytes. *Proc Natl Acad Sci USA* 79, 5921-5925 (1982).

19. J.L. Carpentier, H. Gazzano, E.V. Obberghen, M. Fehlmann, P. Freychet, and L. Orci: Intracellular pathway followed by the insulin receptor covalently coupled to ^{125}I-photoreactive insulin during internalization and recycling. *J. Cell Biol.* 102, 989-996 (1986).

20. R. Rabkin, G.M. Reaven, and C.E. Mondon: Insulin metabolism by liver, muscle, and kidneys from spontaneously diabetic rats. *Am. J. Physiol.* 250, E530-E537 (1986).

21. D.C. Whitcomb, T.M. O'Doriso, S. Cataland, M.A. Shetzline, and M.T. Nishikawara: Identification of tissue insulin receptors: Use of a unique in vivo radioreceptor assay. *Am. J. Physiol.* 249, E561-E567 (1985).

22. H. Sato, Y. Sugiyama, Y. Sawada, T. Iga, and M. Hanano: Binding of radioiodinated human β-endorphin to serum proteins from rats and humans, determined by several methods. *Life Sci.* 1985, 1309-1318 (1985).

23. E. Wisse, De R. Zanger, K. Charels, P.V.D. Smissen, and R.S. McCuskey: The liver sieve. Consideration concerning the structure and function of endothelial fenestrae, the sinusoidal wall, and the space of Disse. *Hepatology (Baltimore)* 5, 683-692

(1985).

24. H.S.G. Chen and J.F. Gross: Estimation of tissue-to-plasma partition coefficients used in physiological pharmacokinetic models. *J. Pharmacokin. Biopharm.* 7, 117-125 (1979).

25. R.J. Lutz, R.L. Dedrick, and D.S. Zaharko: Physiological pharmacokinetics: An in vivo approach to membrane transport. *Pharmacol. Ther.* 11, 559-592 (1980).

26. C.M. Metzler, G.L. Elfring, and A.J. McEwen: A package of computer programs for pharmacokinetic modeling. *Biometrics* 30, 562-(1974).

27. B. Desbuquois, S. Lopez, and H. Burlet: Ligand-induced translocation of insulin receptors in intact rat liver. *J. Biol. Chem.* 257, 10852-10860 (1982).

28. R. Vigneri, N.B. Pilam, D.C. Cohen, V. Pezzino, K.Y. Wong, and I.D. Goldfine: In vivo regulation of cell surface and intracellular insulin binding sites by insulin. *J. Biol. Chem.* 253, 8192-8197 (1978).

29. J.M. Olefsky and M. Kao: Surface binding and rates of internalization of ^{125}I-insulin in adipocytes and IM-9 lymphocytes. *J. Biol. Chem.* 257, 8667-8673 (1982).

30. M.L. Standaert and R.J. Pollet: Equilibrium model for insulin-induced receptor down-regulation. Regulation of insulin receptors in differentiated BC3H-1 myocytes. *J. Biol. Chem.* 259, 2346-2354 (1984).

31. E. Rasio: The capillary barrier to circulating insulin. *Diabetes Care* 5, 158-161 (1982).

32. S.S. Chernick, R.J. Gardiner, and R.O. Scow: Restricted passage of

insulin across capillary endothelium in perfused rat adipose tissue. *Am. J. Physiol.* **253**, E475-E480 (1987).

33. D.E. James, K.M. Burleigh, and E.W. Kraegen: Time dependence of insulin action in muscle and adipose tissue in the rat in vivo. An increasing response in adipose tissue with time. *Diabetes* **34**, 1049-1054 (1985).
34. I. Jialal, G.L. King, S. Buchwald, R. Kahn, and M. Crettaz: Processing of insulin by bovine endothelial cells in culture. Internalization without degradation. *Diabetes* **33**, 794-800 (1984).
35. K. Dernovsek and R.S. Bar: Processing of cell-bound insulin by capillary and macrovascular endothelial cells in culture. *Am. J. Physiol.* **248**, E244-E251 (1985).
36. D.K. Reed, C. Newton, M. Fraga, K. Glastad, A. Bagheri, S. Harris, and B.C. Reed: An analysis of the relationship between the cellular distribution and the rate of turnover for the separate classes of unoccupied, noncovalently occupied, and covalently occupied insulin receptor. *J. Biol. Chem.* **264**, 12673-12679 (1989).
37. J.R. Levy and J.M. Olefsky: The trafficking and processing of insulin and insulin receptors in cultured rat hepatocytes. *Endocrinology* **121**, 2075-2086 (1987).
38. W.M. Pardridge, J. Eisenberg, and J. Yang: Human blood-brain barrier insulin receptor. *J. Neurochemistry* **44**, 1771-1778 (1985).
39. W.K. Morishige, C.A. Uetake, F.C. Greenwood, and J. Akaka: Pulmonary insulin responsivity: In vivo effects of insulin on the diabetc rat lung and specific insulin binding to lung

receptors in normal rats. *Endocrinology* **100**, 1710-1722 (1976).

40. D.M. Geddes, J.P. Blackburn, J.S. Bailey, and F.J. Muller: Effects of pulmonary circulation on blood levels of insulin and glucagon in ambulant dogs. *J. Appl. Physiol.* **46**, 593-598 (1979).
41. R. Rabkin, M.P. Ryan, and W.C. Duckworth: The renal metabolism of insulin. *Diabetologia* **27**, 351-357 (1984).
42. O. Nagata, M. Murata, H. Kato, T. Terasaki, H. Sato, and A. Tsuji: Physiological pharmacokinetics of a new muscle-relaxant, Inaperisone, combined with its pharmacological effect on blood flow rate. *Drug Metab. Dispos.* **18**, 902-910 (1990).
43. K.B. Bishoff and R.L. Dedrick: Thiopental pharmacokinetics. *J. Pharm. Sci.* **57**, 1346-1351 (1968).
44. A. Tsuji, T. Terasaki, N. Imaeda, K. Nishide, and I. Tamai: Age-related change in tissue-to-plasma partition coefficient of cefazolin for noneliminating organs in the rat. *J. Pharm. Sci.* **78**, 535-540 (1989).
45. E. Okezaki, T. Terasaki, M. Nakamura, O. Nagata, H. Kato, and A. Tsuji: Structure-tissue distribution relationship based on physiological pharmacokinetics for NY-198, a new antimicrobial agent, and the related pyridonecarboxylic acids. *Drug Metab. Dispos.* **16**, 865-874 (1988).

(Continued for Table 1)

[c] Measured using ^{14}C-inulin in mice (for details, see text).

[d] The sum of plasma flow rates in all tissues except for the lung, spleen, and gut.

[e] Cited from ref. 45 with correction for body weight.

[f] Cited from ref. 9, with correction for body weight.

[g] The P of inulin across the BBB was not considered, while those in the liver and spleen were assumed to be very high compared with blood flow rates.

TABLE 1

Physiological constants (V_T, V_{CB}, Q_p, V^{IS}), tissue-to-plasma concentration ratios ($K_{p,inu}$), and vascular permeability clearances (P) of ^{14}C-inulin for a 35-g mouse

Tissue	V_T[a]	V_{CB}[b]	Q_p	V_{IS}[c]	$K_{p,inu}$	P[b]
	ml	*ml*	*ml/min*	*ml*		*ml/min*
Venous plasma	0.420[b]	0.420	3.24[d]	-	-	-
Arterial plasma	0.220[b]	0.220	3.24[d]	-	-	-
Lung	0.234	0.042	3.24[d]	0.0454	0.194	0.0255
Brain	0.168[e]	0.00196[f]	0.0840[e]	0.00468	0.0279	-[g]
Heart	0.140	0.028	0.116	0.0188	0.134	0.00591
Skin	6.27	0.028	0.350	1.53	0.244	0.162
Muscle	15.8	0.098	0.532	2.31	0.146	0.418
Liver	1.54[e]	0.140	1.13[e]	0.550	0.357	-[g]
Spleen	0.140[e]	0.0118	0.0280[e]	0.0375	0.268	-[g]
Gut	2.34	0.434	0.378	0.373	0.159	0.154
Kidney	0.280[e]	0.364	0.882[e]	0.0588[b]	0.210	0.370
Adipose	1.40[f]	0.00553[f]	0.140[f]	0.100	0.0714	0.0316

[a] Cited from ref. 44, unless otherwise described in the footnote, with correction for body weight.

[b] Cited from ref. 10, with correction for body weight.

(To be continued)

TABLE 2

Tissue-to-plasma concentration ratios (K_p and $K_{p,ns}$), unbound fractions in the ISF (f_{IS} and $f_{IS,ns}$), nonspecific binding constant (α), and specific binding capacity (R_S/V_T) of A_{14}-^{125}I-insulin for a 35-g mouse

Tissue	K_p[a]	$K_{p,ns}$[a]	f_{IS}[b]	$f_{IS,ns}$[b]	α[c]	R_S/V_T[c]
						pmol/g wt.
Lung	0.805	0.196	0.210	0.862	0.160	0.521
Brain	0.0253	0.0166	-[d]	-[d]	0.476	0.00744
Heart	0.407	0.132	0.287	0.886	0.129	0.235
Skin	0.179	0.133	1.0	1.0	0	0
Muscle	0.181	0.139	0.706	0.919	0.0881	0.0359
Liver	-	0.346	-	0.899	0.112	5.60[e]
Spleen	0.715	0.215	0.326	1.0	0	0.411
Gut	0.648	0.178	0.214	0.780	0.282	0.402
Kidney	-[f]	-[f]	0.0920[g]	0.0362[g]	26.6	2.63
Adipose	0.149	0.111	0.418	0.560	0.784	0.0325

[a] Calculated from $K_{p,app}$ using equations derived in a previous study (9), except for using eq. 25 for the brain.

[b] Calculated from K_p (or $K_{p,app}$) using eq. 18.

[c] Calculated using the method described in Appendix II.

[d] The f_{IS} in the brain was not defined, because the transcytosis of insulin across the BBB was neglected.

[e] Predicted by the present physiological model (fig. 2) including the "receptor recycling model" (Model A in fig. 1) in the liver.

[f] Not determined, because the observed C_T contains insulin taken up from the luminal side of tubules and that remaining within the tubules.

[g] Estimated by a nonlinear least-squares regression analysis (26).

FIGURE LEGENDS

Fig. 1. *Schematic representation of one-organ models for insulin.*

Models A-E correspond to the liver, kidneys, noneliminating tissues (except for the spleen and brain), spleen, and brain, respectively. Model A presents a "receptor-recycling model" developed recently (19), which includes the known processes of insulin-receptor interaction, RME, intracellular degradation of insulin, return of internalized receptors back to the surface and spontaneous internalization of unoccupied surface receptors. In the liver, the total receptor number (R_T) and dissociation constants (K_d) were set at 8.66 pmol per g liver and 0.5 nM, respectively, and the rate constants of k_{on}, k_{off}, k_{end}, k_{sp}, k_{ret}, and k_{deg} were 2.4 x 10^8 $min^{-1} \cdot M^{-1}$, 0.12 min^{-1}, 0.62 min^{-1}, 0.022 min^{-1}, 0.11 min^{-1} and 0.907 min^{-1}, respectively, as calculated or estimated in the previous study (4). In model B, insulin unbound in plasma is filtered at the glomeruli, followed by reabsorption and enzymatic degradation in the proximal tubules, as previously suggested (41). In models B-E, the equilibrium receptor binding and vascular permeability clearance of insulin were incorporated. For abbreviation and symbols, see Appendix I.

Fig. 2. *Schematic diagram of a physiologically based pharmacokinetic model for insulin in mice.*

The "receptor-recycling model" (Model A in fig. 1) is incorporated into the liver, and the vascular permeability and the equilibrium receptor binding of insulin are incorporated in the extrahepatic tissues as well.

Fig. 3. *Predicted and observed ^{14}C-inulin concentrations in plasma and*

in various tissues after iv bolus injection in mice.

The concentration (% dose/ml) of ^{14}C-inulin in plasma and in various tissues were examined at designated times after the iv injection of a tracer dose of ^{14}C-inulin (approximately 6.5 μCi/kg) in mice. Each point and vertical bar represent the mean and SE from 3-5 mice. Solid lines show the predicted curves based on the "capillary-limited" physiological pharmacokinetic model described previously (11-13).

Fig. 4. *Predicted and observed A_{14}-^{125}I-insulin concentrations in plasma and in various tissues after iv bolus injection in mice at a low dose.*

The concentration (% dose/ml) of A_{14}-^{125}I-insulin in plasma and in various tissues were examined at designated times after iv injection at a tracer dose of A_{14}-^{125}I-insulin (approximately 6.5 μCi/kg) in mice. Each point and vertical bar represent the mean and SE from 3-5 mice. Solid lines show the predicted curves based on the physiological pharmacokinetic model shown in fig. 2.

Fig. 5. *Predicted and observed A_{14}-^{125}I-insulin concentrations in plasma and in various tissues after iv bolus injection in mice at a high dose.*

The concentration (% dose/ml) of A_{14}-^{125}I-insulin in plasma and in various tissues were examined at designated times after iv injection at a tracer dose of A_{14}-^{125}I-insulin (approximately 6.5 μCi/kg) plus large excess amount of unlabeled insulin (8 U/kg) in mice. Each point and vertical bar represent the mean and SE from 3-5 mice. Solid lines show the predicted curves based on the physiological pharmacokinetic model shown in fig. 2.

Fig. 6. *Prediction of the changes in the amounts of insulin bound to receptors, internalized, and unbound in the ISF, and of the changes in the numbers of the surface and intracellular receptors in the liver, after iv injection at low and high doses in mice.*

Panels A and C represent the changes in the amounts (pmol per liver) of insulin bound to surface receptors (solid lines), internalized (broken lines), and unbound in the ISF (dotted lines) at low and high doses, respectively. Panels B and D represent the changes in the numbers of surface (solid lines) and intracellular receptors (broken lines) at low and high doses, respectively.

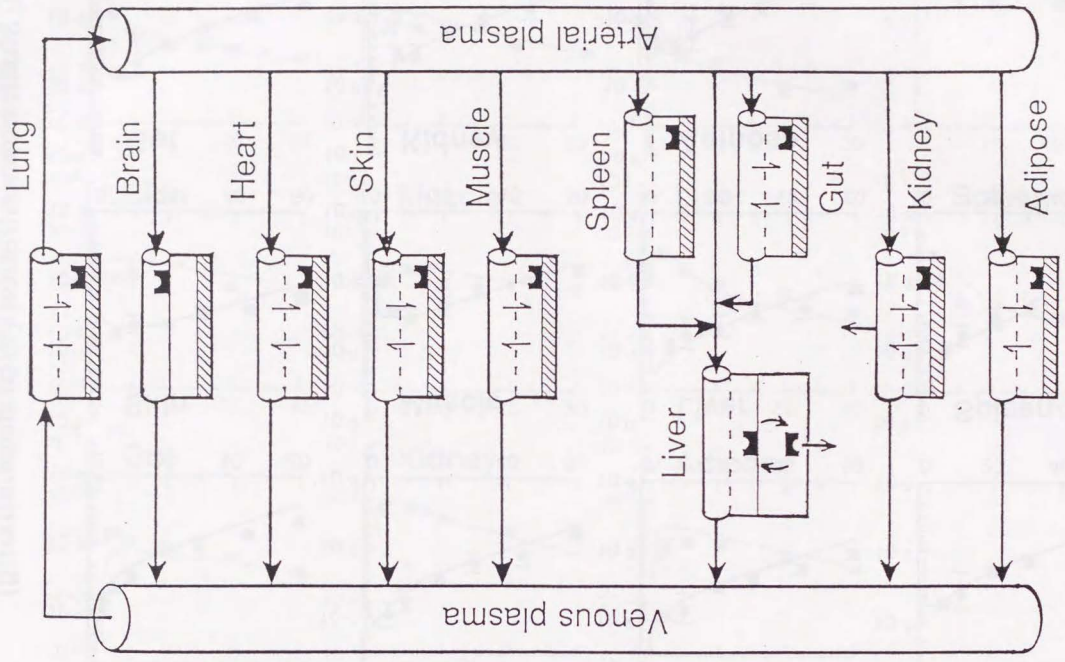
Arterial plasma
Lung
Brain
Heart
Skin
Muscle
Spleen
Gut
Kidney
Adipose
Liver
Venous plasma

Fig. 2

Fig. 1

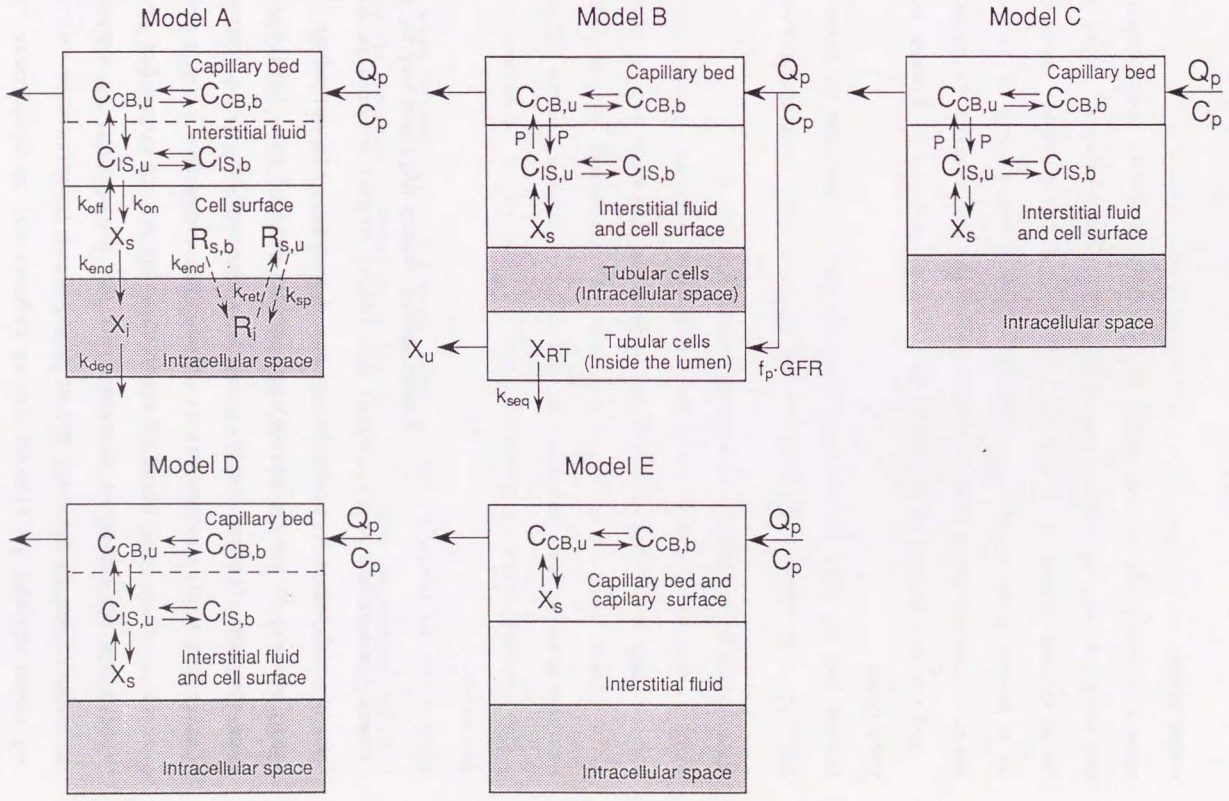
Model A
Capillary bed
$C_{CB,u} \rightleftarrows C_{CB,b}$
Q_p
C_p
Interstitial fluid
$C_{IS,u} \rightleftarrows C_{IS,b}$
k_{off}
k_{on}
Cell surface
X_s
$R_{s,b}$
$R_{s,u}$
k_{end}
k_{end}
k_{ret}
k_{sp}
X_i
R_i
k_{deg}
Intracellular space
Model B
Capillary bed
$C_{CB,u} \rightleftarrows C_{CB,b}$
Q_p
C_p
P
P
$C_{IS,u} \rightleftarrows C_{IS,b}$
X_s
Interstitial fluid and cell surface
Tubular cells (Intracellular space)
X_u
X_{RT}
Tubular cells (Inside the lumen)
$f_p \cdot GFR$
k_{seq}
Model C
Capillary bed
$C_{CB,u} \rightleftarrows C_{CB,b}$
Q_p
C_p
P
P
$C_{IS,u} \rightleftarrows C_{IS,b}$
X_s
Interstitial fluid and cell surface
Intracellular space
Model D
Capillary bed
$C_{CB,u} \rightleftarrows C_{CB,b}$
Q_p
C_p
$C_{IS,u} \rightleftarrows C_{IS,b}$
X_s
Interstitial fluid and cell surface
Intracellular space
Model E
$C_{CB,u} \rightleftarrows C_{CB,b}$
Q_p
C_p
X_s
Capillary bed and capilary surface
Interstitial fluid
Intracellular space

Fig. 4

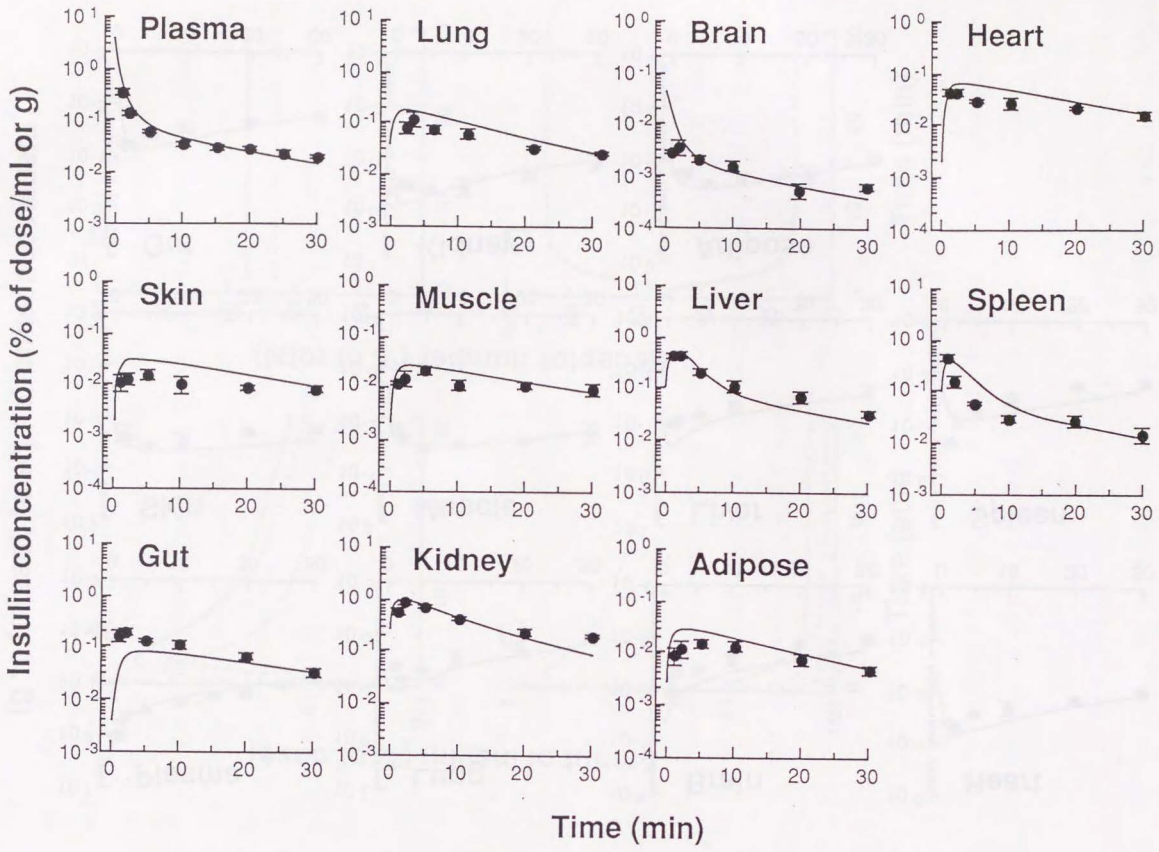
Plasma
Lung
Brain
Heart
Skin
Muscle
Liver
Spleen
Gut
Kidney
Adipose
Insulin concentration (% of dose/ml or g)
Time (min)

Fig. 3

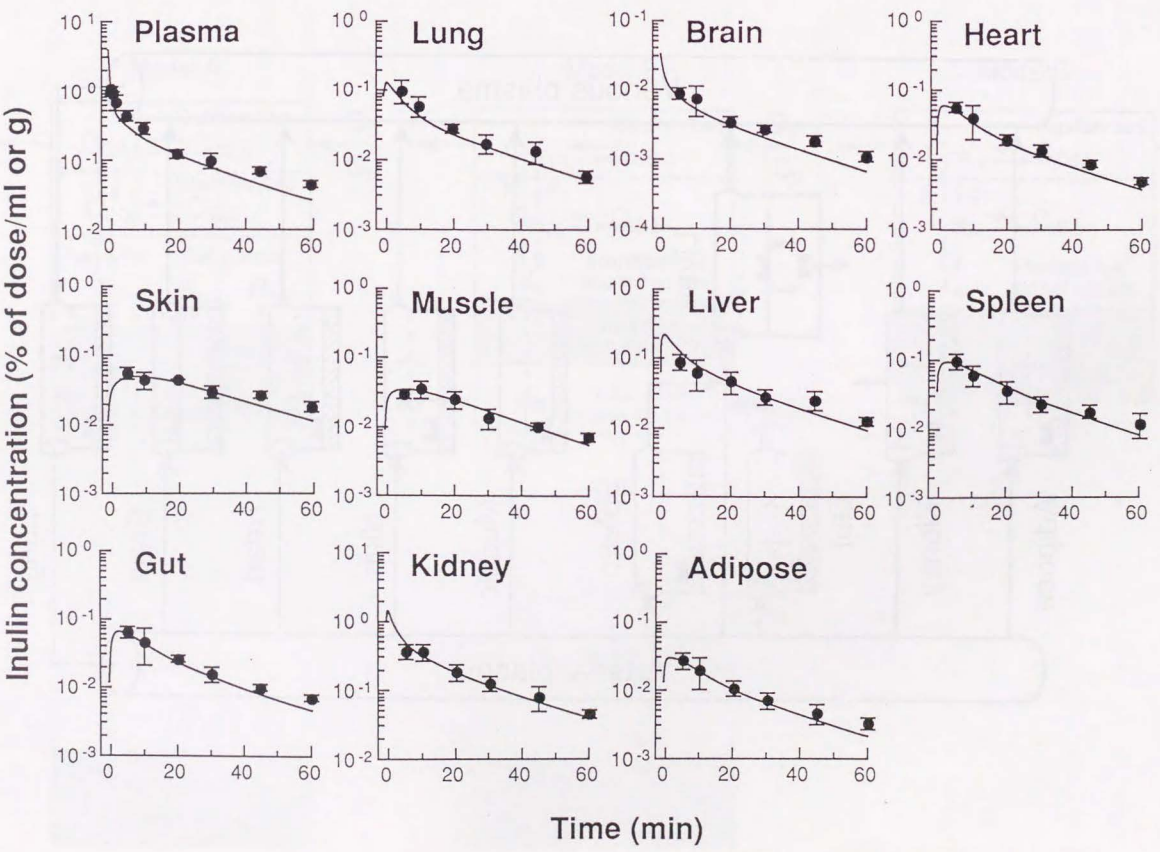
Plasma
Lung
Brain
Heart
Skin
Muscle
Liver
Spleen
Gut
Kidney
Adipose
Inulin concentration (% of dose/ml or g)
Time (min)

Fig. 5

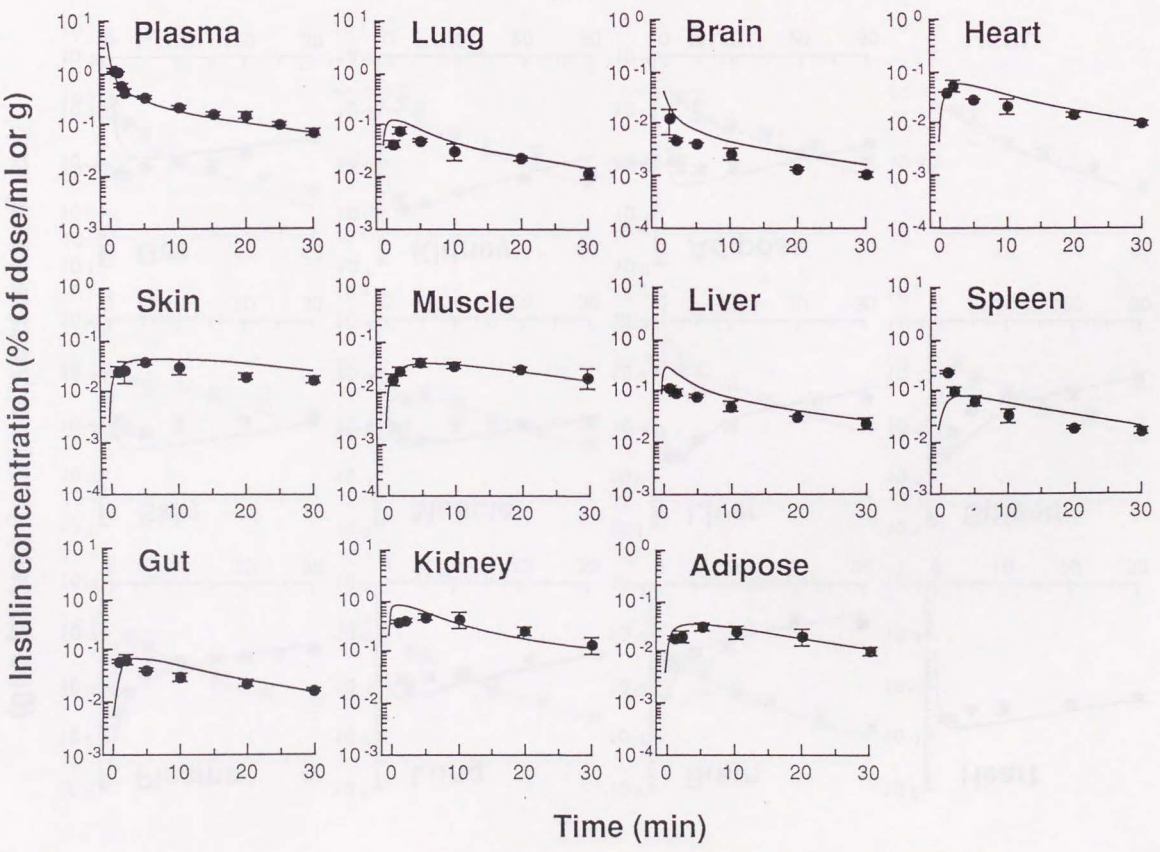
Plasma
Lung
Brain
Heart
Skin
Muscle
Liver
Spleen
Gut
Kidney
Adipose
Insulin concentration (% of dose/ml or g)
Time (min)

Fig. 6

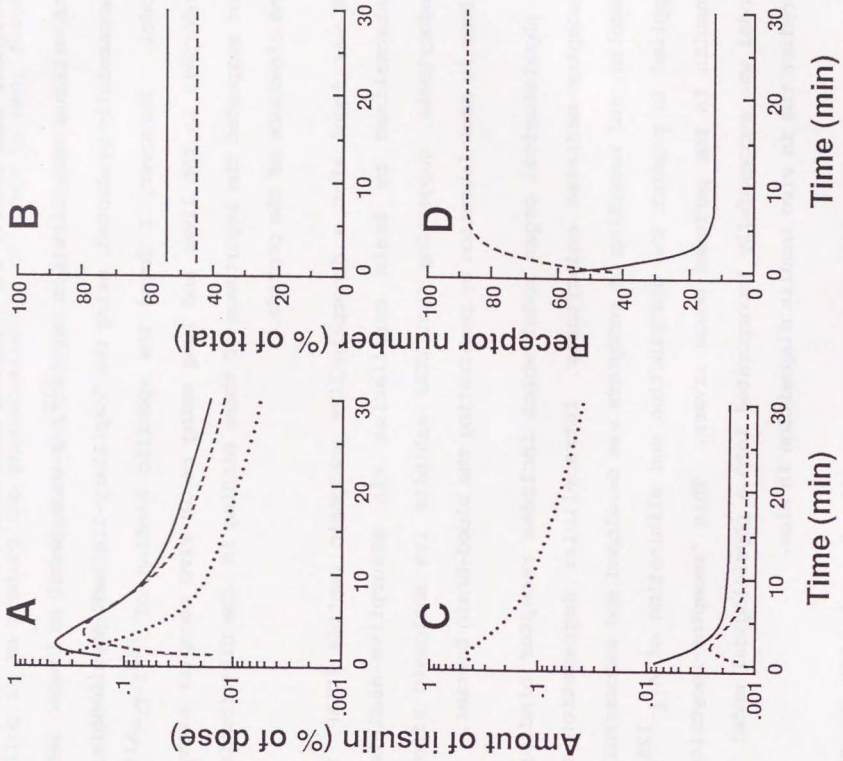
A
B
C
D
Amout of insulin (% of dose)
Receptor number (% of total)
Time (min)
Time (min)

CONCLUSIONS AND PERSPECTIVES

Throughout this thesis, the following conclusions were obtained:

1) The tissue distribution of ^{125}I-β-endorphin in rats was successfully predicted, using the "capillary-limited" physiological model. Moreover, I found the specific binding of ^{125}I-Tyr^{A14}-endorphin in the liver and lung using an *in vivo* receptor assay, and suggested the importance of these binding in the distribution and clearance of the peptide.

2) It was found that a dynorphin-like analgesic peptide (DLAP) is internalized by brain capillaries *via* adsorptive-mediated endocytosis, suggesting that DLAP exhibits its analgesic effect after iv administration by penetrating the blood-brain barrier.

3) A physiological organ model which includes receptor binding, receptor-mediated endocytosis, intracellular degradation of insulin, and recycling of receptors was developed and successfully applied to predict the distribution and elimination of A_{14}-^{125}I-insulin in the perfused mouse livers. This "receptor-recycling" model was successfully incorporated into a physiological model to predict the *in vivo* insulin disposition in mice.

Thus, important roles of receptor-mediated processes on the pharmacokinetics of peptide hormones were clarified in a physiological context. The methods and principles developed here can be applied to other biologically active peptides, with adequate modifications of the model. Since the "receptor-recycling model" could also predict the changes in surface receptor number in target tissues, a quantitative

prediction of *in vivo* insulin efficacy might be performed using this model in the future. Moreover, since a final goal of physiological modeling is to predict the pharmacokinetics of drugs in man, future studies should be directed to the scale-up of insulin pharmacokinetics from animal to human.

Fundamentals of Optical Fiber Sensors